remote sensing

MDPI

Article

Burned Areas Mapping Using Sentinel-2 Data and a Rao's Q Index-Based Change Detection Approach: A Case Study in Three Mediterranean Islands' Wildfires (2019–2022)

Rafaela Tiengo [1,2], Silvia Merino-De-Miguel [1], Jéssica Uchôa [2], Nuno Guiomar [3,4,5] and Artur Gil [6,*]

[1] Departamento de Ingeniería y Gestión Forestal y Ambiental, ETSIMFMN—Escuela Técnica Superior de Ingeniería de Montes, Forestal y del Medio Natural, Universidad Politécnica de Madrid, 28040 Madrid, Spain; r.dtiengo@alumnos.upm.es (R.T.); silvia.merino@upm.es (S.M.-D.-M.)
[2] cE3c—Centre for Ecology, Evolution and Environmental Changes, Azorean Biodiversity Group, CHANGE—Global Change and Sustainability Institute, University of the Azores, 9500-321 Ponta Delgada, Portugal; jessica.uchoa@parceiros.nos-acores.pt
[3] MED—Mediterranean Institute for Agriculture, Environment and Development, CHANGE—Global Change and Sustainability, University of Évora-PM, Apartado 94, 7006-554 Évora, Portugal; nunogui@uevora.pt
[4] EaRSLab—Earth Remote Sensing Laboratory, University of Évora-CLV, Rua Romão Ramalho, 59, 7000-671 Évora, Portugal
[5] IIFA—Institute for Advanced Studies and Research, University of Évora-PV, Largo Marquês de Marialva, Apartado 94, 7002-554 Évora, Portugal
[6] IVAR—Research Institute for Volcanology and Risk Assessment, University of the Azores, 9500-321 Ponta Delgada, Portugal
* Correspondence: artur.jf.gil@uac.pt

Abstract: This study explores the application of remote sensing-based land cover change detection techniques to identify and map areas affected by three distinct wildfire events that occurred in Mediterranean islands between 2019 and 2022, namely Sardinia (2019, Italy), Thassos (2022, Greece), and Pantelleria (2022, Italy). Applying Rao's Q Index-based change detection approach to Sentinel-2 spectral data and derived indices, we evaluate their effectiveness and accuracy in identifying and mapping burned areas affected by wildfires. Our methodological approach implies the processing and analysis of pre- and post-fire Sentinel-2 imagery to extract relevant indices such as the Normalized Burn Ratio (NBR), Mid-infrared Burn Index (MIRBI), Normalized Difference Vegetation Index (NDVI), and Burned area Index for Sentinel-2 (BAIS2) and then use (the classic approach) or combine them (multidimensional approach) to detect and map burned areas by using a Rao's Q Index-based change detection technique. The Copernicus Emergency Management System (CEMS) data were used to assess and validate all the results. The lowest overall accuracy (OA) in the classical mode was 52%, using the BAIS2 index, while in the multidimensional mode, it was 73%, combining NBR and NDVI. The highest result in the classical mode reached 72% with the MIRBI index, and in the multidimensional mode, 96%, combining MIRBI and NBR. The MIRBI and NBR combination consistently achieved the highest accuracy across all study areas, demonstrating its effectiveness in improving classification accuracy regardless of area characteristics.

Keywords: remote sensing; wildfire; burned areas; Sentinel-2; Rao's Q index; vegetation indices

Academic Editors: Michael Sprintsin and Wenjiang Huang

Received: 15 December 2024
Revised: 23 February 2025
Accepted: 25 February 2025
Published: 27 February 2025

Citation: Tiengo, R.; Merino-De-Miguel, S.; Uchôa, J.; Guiomar, N.; Gil, A. Burned Areas Mapping Using Sentinel-2 Data and a Rao's Q Index-Based Change Detection Approach: A Case Study in Three Mediterranean Islands' Wildfires (2019–2022). *Remote Sens.* **2025**, *17*, 830. https://doi.org/10.3390/rs17050830

1. Introduction

Fire is an ecological process and the main ecosystem disturbance in most of the world's ecosystems [1,2], shaping species traits, vegetation communities, and landscapes [3–10]. Fires are driven by interactions between vegetation (fuel complexes), fire weather, and

topography [11]. The variability in the relationships between these factors determines the existence of different patterns in the spatial and temporal distribution of fire characteristics, the relative importance of their drivers, and their impacts on ecological and socio-ecological systems. This variability allows for the identification and characterization of distinct fire regimes across the globe (e.g., [12–14]). However, fire regimes are dynamic and respond to shifts in vegetation and climate patterns (e.g., as these environmental factors continue to evolve due to climate change, fire activity is expected to intensify in the coming decades [15,16], driven by increased fuel availability and more extreme weather conditions).

While there is a global decrease in the burned area [17], this does not invalidate the existence of opposite trends in specific regions (e.g., [18]). However, an increase in the frequency of extreme fires is currently being observed [19]. Records of catastrophic fire seasons are thus becoming more common (e.g., [20,21]), with a high number of fatalities (e.g., [22,23]) and extensive damage to properties and structures (e.g., [24,25]). These extreme fires continue to challenge the resilience thresholds of affected ecosystems, even in fire-prone regions where communities have evolved with fire and developed fire-related traits, inducing significant changes in plant communities and the landscape [26].

Coastal areas and islands are particularly vulnerable to these extreme events. In August 2023, a series of wind-driven fires spread on the island of Maui, Hawaii, intensified by Hurricane Dora, killing more than 100 people and generating estimated losses of USD 5.5 billion [27]. Another catastrophic event occurred in July 2018 in the Attica region of Greece, when the fire started on Mount Pentelli reached the east coast (Mati) driven by katabatic winds, trapping hundreds of people, causing the deaths of more than 100, injuring more than 150, and destroying about 1650 buildings [28,29]. In August 2007, a group of 12 firefighters died in a fire that occurred on Kornat Island in Croatia after being trapped by a sudden change in the fire's behavior [30]. This followed the deaths of three firefighters in July of the same year in similar conditions during the fire of Doxaro on the island of Crete in Greece [31]. Couto et al. [32] identified the patterns of atmospheric conditions and orographic effects that drove a series of large fires on Madeira Island between 2010 and 2016, which expanded quickly and reached wildland–urban interfaces, threatening people and destroying structures. In Italy, wildfire activity has been rising in recent years, with the most significant contributions to this increase coming from fires on the islands of Sicily and Sardinia, being particularly relevant to the larger fires in 2007, 2017, and 2021 [33,34].

Despite this susceptibility and vulnerability to fire, the evolution of its contemporary regime on islands is not well understood, and this gap is highlighted by Badeau et al. [35] and Molina-Terrén et al. [36], who analyzed the evolution of the fire regime in the western Canary Islands (Macaronesia) and Corsica (Mediterranean), respectively. Despite the different geographic contexts, the authors' results were similar, emphasizing the pernicious effects of fire suppression policies on regime shifts toward less frequent but larger and more severe fires.

This shift contributed to the firefighting trap observed in other mainland fire-prone regions [37–40] and required changes to fire and landscape management policies [41]. However, although the general principles for implementing sustainable fire management systems may be the same everywhere [42–44], the effectiveness of implementing fire-smart strategies at regional and local scales depends on each specific context and its adaptation to the present and future fire regime [44–50]. Therefore, systematic monitoring and mapping of burned areas are critical to achieving success, as pointed out by Roy et al. [27] following the devastating wildfires on Maui Island (Hawaii). The periodic recording of burned areas allows fire scientists and practitioners to increase their understanding of extreme events by establishing a baseline for their spatiotemporal evolution [51]. Furthermore, since fire is a self-regulating process [52], it is crucial to gather information for the tactical resources

involved in fire suppression about new fire attack opportunities created by recent events, which also allows fire planners to re-set fire prevention priorities.

The usefulness of remote sensing data for detecting and monitoring active fires, mapping burned areas, assessing fire severity, and monitoring post-fire vegetation response is undeniable [53,54]. However, there are still several challenges to overcome and new achievements to be considered despite the efforts of science and the countless techniques developed to detect burned areas around the world [27,55]. Global burned area products derived from coarse spatial resolution sensors (e.g., [56–63]) are an essential source of information for the fire science community, allowing for the identification of different fire regimes at global and continental scales (e.g., [12,64]), or as a baseline to compute spatiotemporal metrics of fire dynamics (e.g., [65]), which are particularly relevant to understanding the drivers of infrequent but extreme events. Despite the usefulness of global burned area products, the assessment of their accuracy (e.g., [66,67]) revealed commission and omission errors exceeding those required for the fulfillment of some specific objectives, such as climate modeling [68]. The higher omission error values are partly due to the failure to detect small fires caused by low spatial resolution [69–71], an underestimation that can be particularly significant in some pyro-regions not only in terms of the total amount of burned area (e.g., [72]), but also in regard to the contribution of these small fires to the maintenance a pyro-diverse mosaic in the landscape that limits the spread of large fires (e.g., [73]), or their relevance in estimating global fire effects (e.g., global fire emissions estimated by [74] increased by 11% compared to previous estimates [75] as a result of improvements in the estimation of burned areas).

Using data from medium-resolution sensors makes it possible to overcome the aforementioned limitations and map small fires, spatially scattered and showing complex shapes. Landsat data have been used extensively to map burned areas with better accuracy (e.g., [76–81]), particularly after the change in distribution policy in 2008 that allowed free access to users [82], since they have better spatial resolution (30 m after the launch of the Thematic Mapper (TM) Landsat sensor in 1982; [83,84]) and allow long-term time series of burned areas relevant for detecting spatial and temporal trends and patterns [85–88] However, the 16-day temporal resolution limits the accuracy of products derived from these images, particularly in areas with high persistence of cloud cover and territories where the burned area persistence time is short [72,89,90], such as grasslands and savannas (e.g., [91,92]). Since the deployment of Sentinel-2A in 2015 and Sentinel-2B in 2017, their imagery has seen growing use in mapping and analyzing areas affected by fires [33,72,93–99], given their better spatial (10/20 m) and temporal (global mean and median average revisit intervals of 3.8 and 3.7 days) resolution [100]

However, despite improvements in spatial, temporal, and spectral resolution, methodological challenges persist in detecting burned areas (e.g., [101]). There are still some important sources of commission errors that result in overestimates of the burned area (e.g., [102]), which arise from similarities in the spectral and/or temporal patterns with the burned areas, such as particular land cover types (e.g., croplands), other disturbances (e.g., logging), or the presence of shadows (e.g., from clouds or topography) (e.g., [77,103]). Therefore, the choice of spectral indices to use to detect burned areas can have a significant influence on the final result. The NBR index integrates the NIR and SWIR bands in its calculation and is one of the most widely used metrics in assessing fire severity (e.g., [104–106]) and in mapping burned areas (e.g., [107–109]). For example, the MIRBI index was developed for application in savannah ecosystems where the relevance of NIR wavelengths is lower due to the senescent state of vegetation at the end of the fire season [110]. The NDVI has limitations in low primary productivity landscapes and in fire severity estimation and burned areas mapping in regions where the dry period and fires coincide (e.g., [111]), but

it has shown high performance in other contexts, with greater water availability, such as in burned patches in Madeira Island [112]. Thus, the selection of indices depends on the context in which the fires spread, and possible synergies can be explored by integrating various metrics in the analytical process of mapping burned areas.

Another important source of commission errors is the presence of unburned "islands" within burned patches. In fact, the distribution of fire severity in vegetation is spatially heterogeneous within a burned perimeter, and it is complex to distinguish low-severity burned areas from unburned patches. Moreover, the impact of noise and weather conditions induces variations in the spectral signature between temporal sequences of images, further complicating the change detection task. To overcome these limitations, several authors have proposed approaches based on Markov Random Fields (MRF) to detect changes by considering the spatial–contextual information between neighboring pixels, thereby increasing the accuracy of the final map [113–118]. However, in complex landscapes, excessive smoothing in the results obtained through these approaches is a common problem (e.g., [119]) since it is difficult to achieve the optimal balance between detail preservation and noise reduction (e.g., [119]). Several authors have sought to mitigate this problem in MRF approaches by incorporating external knowledge (e.g., [120,121]), integrating local uncertainty parameters (e.g., [120]), and applying adaptive weight functions to the edges (e.g., [115]).

In either case, incorporating spatial information from the neighborhood can lead to a significant improvement in change detection. In this regard, Tassi et al. [122,123] developed a tool that incorporates Rao's Q-diversity index [124], a measure of spatial heterogeneity, to detect land cover changes. It has been applied with good results in detecting changes in different geographic contexts [122,123,125,126] but has never been used to detect burnt areas.

Therefore, the general objective of this study was to test and assess the effectiveness of various indices in detecting and mapping burned areas across different Mediterranean insular regions, namely Sardinia, Thassos, and Pantelleria, using Rao's Q Index-based change detection approaches.

The selection of remote sensing indices used in this study was based on their established effectiveness in detecting and mapping burned areas in various environmental settings. The Normalized Burn Ratio (NBR) and the Mid-infrared Burn Index (MIRBI) were chosen for their sensitivity to fire-induced changes in vegetation and soil reflectance, particularly in the NIR and SWIR spectral regions. The NBR is one of the most used metrics in assessing fire severity (e.g., [104–106]) and in mapping burned areas (e.g., [107–109]). The Normalized Difference Vegetation Index (NDVI) was included for its ability to monitor vegetation health and biomass changes, providing a complementary view of fire damage [112]. Finally, the Burned area Index for Sentinel-2 (BAIS2) was incorporated for its specific design to detect burned areas using Sentinel-2 imagery [127]. The integration of these indices, either individually or in combination, aimed to leverage their specific strengths to improve the accuracy and reliability of burned area detection, particularly in the unique and heterogeneous landscapes of Mediterranean islands.

The process entailed comparing the detection capabilities of each index against established boundaries provided by the Copernicus Emergency Management System (CEMS) and identifying the most effective combinations for accurate burned areas detection and mapping. This comparison explores the use of free and open-source data, such as Sentinel-2 imagery, alongside high-resolution datasets used by CEMS, highlighting the potential of free accessible data sources in wildfire mapping and analysis.

2. Materials and Methods

2.1. Study Areas

Our study was conducted in three Mediterranean insular regions (Figure 1): Sardinia, Thassos, and Pantelleria.

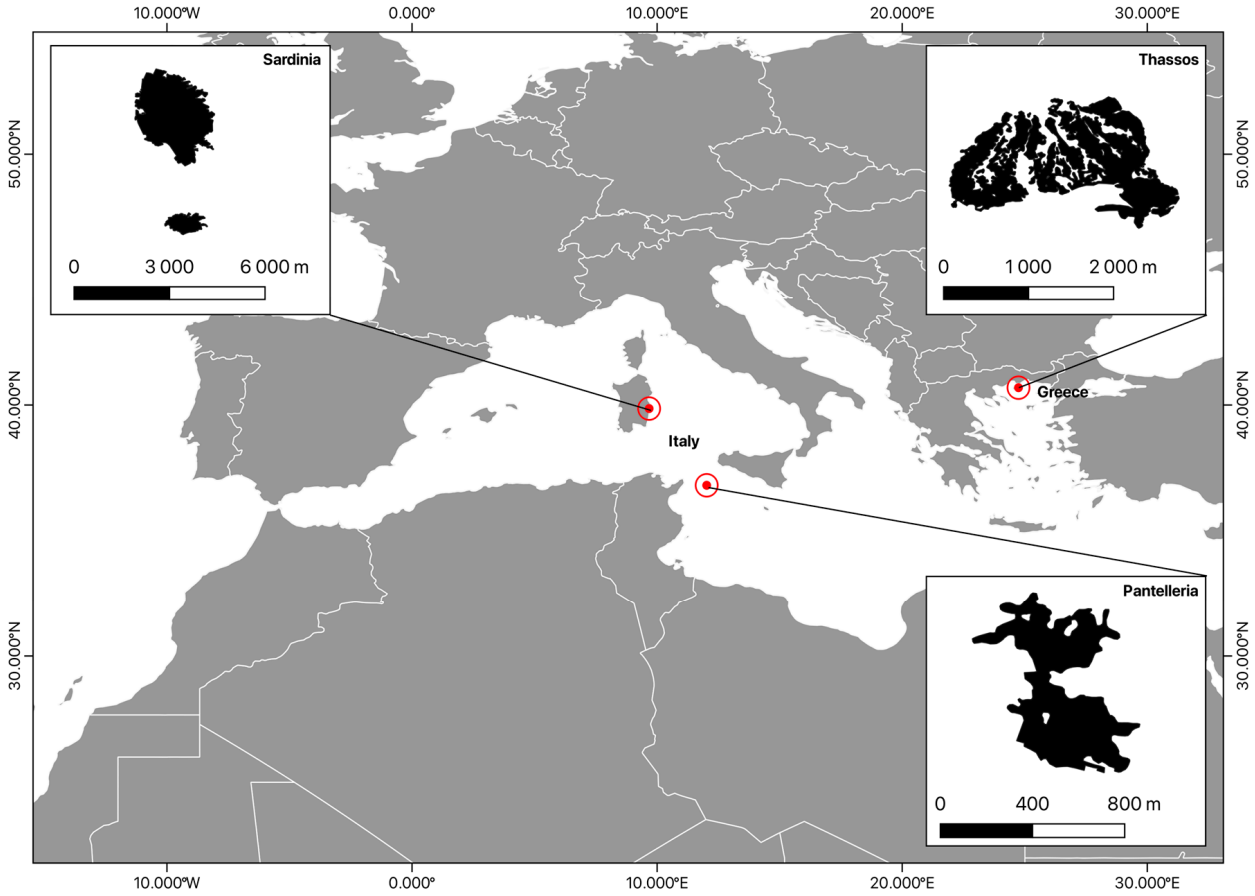

Figure 1. Location of the study areas.

Sardinia, the second-largest island in the Mediterranean Sea (24.090 km^2), exhibits diverse landscapes ranging from mountainous terrain to coastal plains, influencing its susceptibility to wildfires [128,129]. The island's vegetation is dominated by Mediterranean maquis, which includes shrubs, small trees, and herbaceous plants. These vegetation types are highly flammable during the summer months due to prolonged dry conditions. Sardinia's terrain is diverse, with extensive hilly and mountainous areas interspersed with plains, creating varied fire dynamics influenced by wind patterns and topography. The combination of these factors (e.g., dense vegetation, steep slopes, and strong seasonal winds) makes Sardinia particularly vulnerable to wildfires during the summer fire season [128,130].

Pantelleria, a volcanic island between Sicily and Tunisia with an area of 83 km^2, presents a rugged topography and arid climate, posing significant fire risks. The island features a mix of Mediterranean shrubland, small agricultural fields, and terraced olive groves. The volcanic soil provides fertile ground for vegetation, but the dry conditions, combined with strong winds, make Pantelleria susceptible to wildfires. The vegetation is dominated by drought-tolerant shrubs such as junipers and olives, which can ignite and spread fires quickly. Pantelleria has a high biodiversity, hosting several endemic species [131]. Its territory is divided into three bioclimatic belts: (i) inframediterranean semiarid, dominated by maquis; (ii) thermomediterranean dry, with evergreen broadleaf forests; and (iii) mesomediterranean sub-humid, characterized by pine forests [131,132].

Thassos, an island located in the northern Aegean Sea with an area of 378 km^2, is renowned for its rich biodiversity and Mediterranean climate, contributing to its fire-prone ecosystem [133]. Its climate is temperate, warm, and mild, with average temperatures ranging from 5.4 °C (in January) to 26 °C (in July). Summer is characterized by low relative humidity and precipitation. The dominant vegetation includes Aleppo pines and evergreen shrubs, which are highly flammable and contribute to the rapid spread of fire. Thassos' steep slopes and rugged topography further exacerbate fire propagation, making fire suppression efforts challenging [133,134].

Understanding these regions' geographical and environmental context is essential for comprehending the dynamics and impacts of wildfires in each area [135].

2.2. Copernicus Emergency Management Service (CEMS)

Upon an activation request, the CEMS (https://emergency.copernicus.eu/ (accessed on 21 July 2024)) provides high-resolution wildfire maps derived from high-resolution satellite data. These maps are utilized to delineate the perimeters of wildfires and to classify the affected areas into four distinct levels of fire severity [112,127,136,137].

For our three study cases, CEMS employed Pléiades-1A and 1B imagery with a spatial resolution of 0.5 m for Sardinia, PlanetScope imagery with a 3 m spatial resolution for Thassos, and SPOT6 imagery with a 1.5 m resolution for the Pantelleria case study. The key information about the events in the study areas and the CEMS activation is provided in Table 1.

Table 1. Fire event information on the three study areas and the respective Copernicus Emergency Management Service activation codes.

Study Area	Start Date	CEMS Activation	CEMS CODE	Source
Sardinia, Italy	13 July 2019	17 July 2019	EMSR371 (https://mapping.emergency.copernicus.eu/activations/EMSR371/ (accessed on 21 July 2024))	[138]
Thassos, Greece	10 August 2022	17 August 2022	EMSR624 https://mapping.emergency.copernicus.eu/activations/EMSR624/ (accessed on 21 July 2024)	[139]
Pantelleria, Italy	17 August 2022	19 August 2022	EMSR626 https://mapping.emergency.copernicus.eu/activations/EMSR626/ (accessed on 21 July 2024)	[140]

CEMS products were used as a reference. Previous studies have successfully used CEMS data for validation [141]. These products may serve as a viable and reliable alternative to traditional validation measurements, which can require substantial financial, human, and temporal resources. This comparison explores the use of free and open-source data, such as Sentinel-2 imagery, alongside high-resolution datasets used by CEMS, highlighting the potential of free accessible data sources in wildfire mapping and analysis.

Utilizing the outputs from CEMS that delineate the burned areas, an RGB composite of Sentinel-2 images was produced for each study area to enhance the understanding of the affected regions (Figure 2). This approach involves combining different spectral bands (bands 2, 3, and 4 of Sentinel-2) into a single composite image, thereby providing a more comprehensive visual representation of the burned areas.

By integrating the CEMS data with satellite imagery, the analysis not only improves the accuracy of identifying the impacted zones but also enables a more detailed assessment of the extent and severity of the damage. This method proves advantageous in post-event analysis and aids in the efficient allocation of resources for recovery and mitigation efforts.

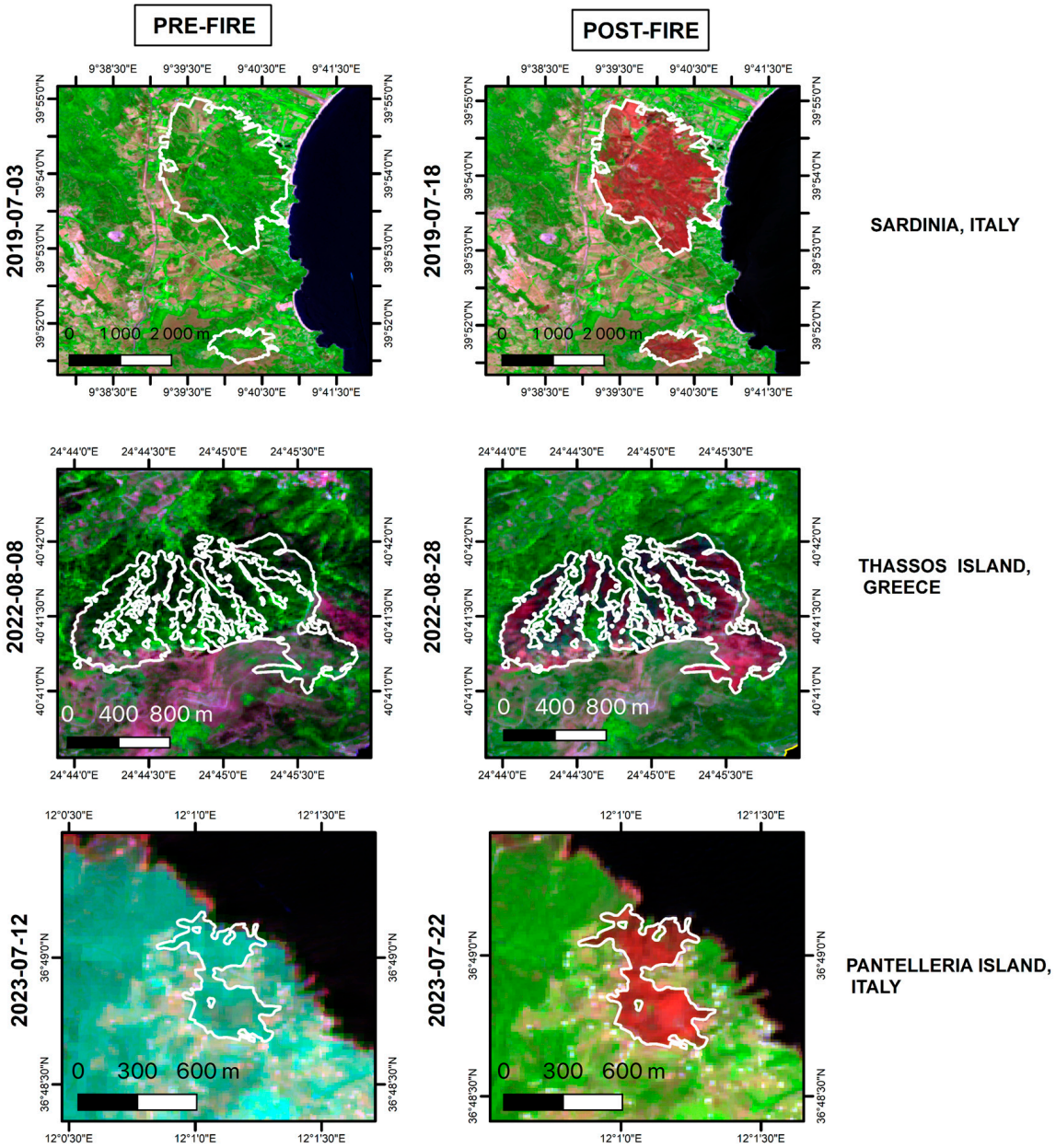

Figure 2. RGB composite image of burned areas based on CEMS outputs delimitation for each study area. Pre-fire Sentinel-2 imagery for Pantelleria shows a slight visual distortion, likely caused by thin cloud cover or minor atmospheric interference during image acquisition. While this can occasionally occur despite atmospheric correction processes, it does not affect the reliability of the subsequent analysis.

2.3. Methods Workflow

This study is primarily based on a Python code developed for an application of Rao's Q index for detecting agricultural land cover changes (available at https://github.com/AndreaTassi23/spectralrao-monitoring, accessed on 1 May 2024) [122] and recently adapted by [125] to identify and assess land use and land cover changes (LULCC) induced by EU-funded conservation projects. Building on these codes, we aimed to retain their basic structure while expanding and adapting their functionalities. Enhancements and new features were introduced to address the emerging demands and needs of our investigation.

This research utilized Google Colab with GEE integration, employing Python 3.10 as the programming language in a stepwise way: (1) accessing the S2 satellite imagery repository on the GEE catalog; (2) extracting the NIR, SWIR, and red bands of the imagery;

(3) applying the Rao's Q classic approach using different spectral indices (MIRBI, NDVI, BAIS2, and NBR); (4) computing the Rao's Q multidimensional using NBR, MIRBI, and NDVI; (5) calculating the square root of the post-image minus the pre-image for each study area; (6) determining the threshold; and (7) validating the results through statistical analysis for each study area, supported by information from reports and historical high-resolution images obtained from satellites and CEMS data (Figure 3).

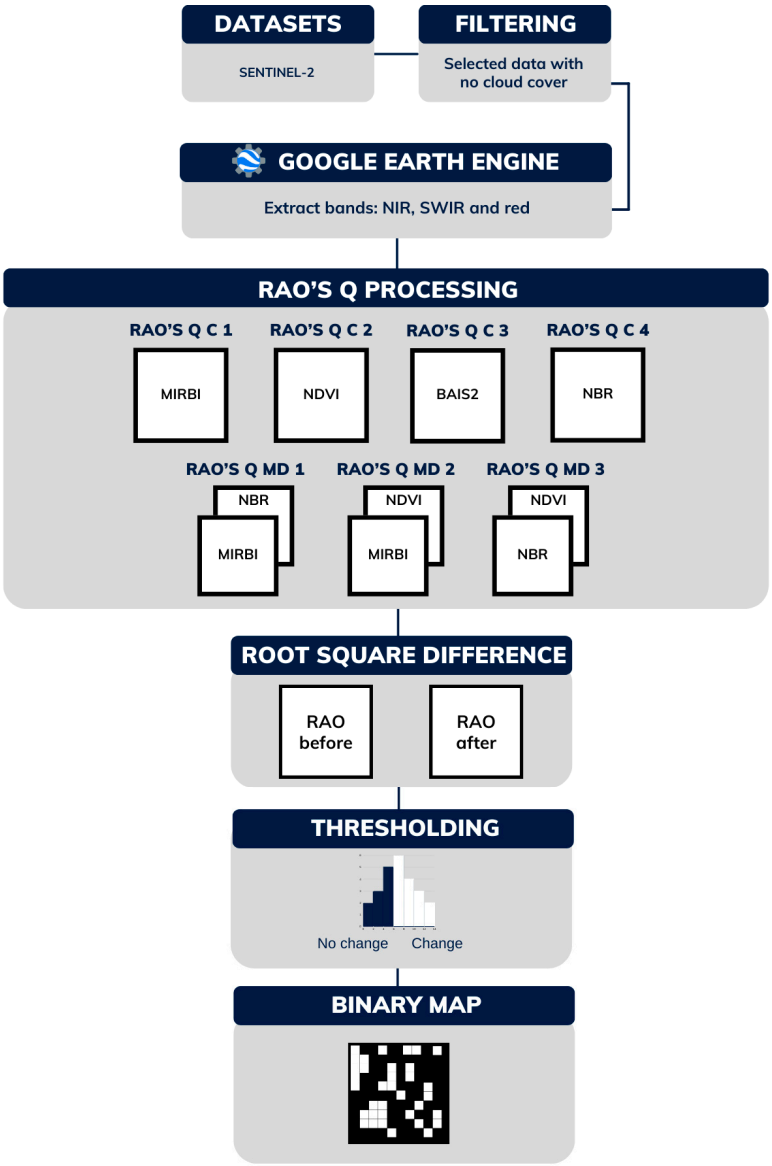

Figure 3. Generic methodological workflow.

Table 2 provides detailed information on the Sentinel-2 imagery utilized in this study, including acquisition dates, study areas, and processing levels. The imagery was sourced from the 'COPERNICUS/S2_SR_HARMONIZED' (available at: https://developers.google.com/earth-engine/datasets/catalog/COPERNICUS_S2_SR_HARMONIZED#description (accessed on 21 July 2024)) collection available on Google Earth Engine, which provides surface reflectance data that have undergone atmospheric correction and harmonization across all Sentinel-2 sensors. This harmonization process ensures consistent radiometric calibration and reduces striping artifacts, making the data suitable for multi-temporal analyses and the calculation of spectral indices used in the methodology.

Table 2. Sentinel-2 imagery acquisition dates for Rao's Q processing in each study area.

Study Area	Date of Event	Pre-Image	Post-Image	Sensor
Sardinia	13 July 2019	3 July 2019	8 July 2019	Sentinel-2
Thassos	10 August 2022	8 August 2022	28 August 2022	
Pantelleria	17 August 2022	13 August 2022	2 September 2022	

The calculation of spectral indices, including NBR, MIRBI, NDVI, and BAIS2, was performed using standard formulas applied to the Sentinel-2 bands. For each index, both pre-fire and post-fire values were computed, resulting in difference maps (Δ-index) to highlight changes caused by the wildfire.

The Rao's Q Index was applied using these difference maps to quantify spatial heterogeneity. Rao's Q calculation involved defining a 9×9 pixel moving window. This approach enabled the identification of areas with significant spectral changes indicative of fire impact.

For the multidimensional approach, combinations of spectral indices were used simultaneously in Rao's Q framework. This required normalizing the indices to ensure comparability across dimensions and calculating Rao's Q Index within the same 9×9 pixel window using a multidimensional distance metric. This enhanced method allowed the analysis to incorporate complementary information from multiple indices, providing a more nuanced representation of fire-induced changes.

The dissimilarity between pre- and post-event Rao's Q maps was quantified through pixel values representing change intensity. For each approach (classic and multidimensional combinations), binary maps were created to classify areas as "change" or "no change". The threshold was determined using a histogram-based method, selecting the point of maximum perpendicular distance from the secant line between the histogram's extremes. This ensured the detection of significant changes while minimizing typical spectral variability.

The GEE platform was used to access Sentinel-2 imagery, while all data processing, index calculations, and Rao's Q analyses were performed in Google Colab using Python. This workflow ensured reproducibility, scalability, and the integration of open-source tools for the entire methodological process.

2.4. Spectral Indices

Following the analysis of Sentinel-2 images, the spectral indices MIRBI, NDVI, BAIS2, and NBR were calculated using the reflectance data from the spectral bands, as specified in Table 3. The reflectance properties of the objects directly impact these values and, therefore, influence the reliability and effectiveness of the spectral indices [142].

Table 3. Spectral indices characterization. The BAIS 2 utilizes two distinct red edge bands (band 6 and band 7), enhancing its sensitivity to vegetation's optical properties variations.

Spectral Index	Equation	Reference
MIRBI (Mid-Infrared Bispectral Index)	$10 * SWIR\,2 - 9.8 * SWIR\,1 + 2$	[92]
NDVI (Normalized Difference Vegetation Index)	$\frac{NIR-Red}{NIR+Red}$	[143]
BAIS2 (Burned area Index for Sentinel-2)	$BAIS2 = \left(1 - \sqrt{\frac{red\ edge\ *red\ edge*NIR}{red}}\right) * \left(\frac{SWIR-NIR}{\sqrt{SWIR+NIR}} + 1\right)$	[33,127]
NBR (Normalized Burn Ratio)	$\frac{(NIR-SWIR)}{(NIR+SWIR)}$	[144,145]

The MIRBI is a crucial remote sensing index designed to detect and assess burned areas. It primarily utilizes spectral bands in the mid-infrared region, particularly the SWIR.

By combining the reflectance values of these bands, the MIRBI provides a robust measure for identifying and quantifying the extent and severity of fire-affected areas. This capability makes it an invaluable tool for environmental monitoring, forest management, and post-fire recovery assessments [72,110].

The NDVI [24] is a widely used index for assessing vegetation vigor and heterogeneity, thereby aiding in identifying potential LULCC [146]. The NDVI is a metric that ranges from −1 to +1. Values approaching +1 generally indicate areas with significant vegetative vigor, while values close to −1 correspond to ice-covered regions. A value of 0 is associated with bare soil [147]. This index is critical in fire mapping [148,149], aiding in monitoring changes in vegetation over time and across different landscapes [146,150,151].

The BAIS2 utilizes vegetation properties characterized within the red-edge spectral regions and the radiometric response in the SWIR spectral range, which is widely acknowledged for its effectiveness in delineating burned areas. This approach harnesses the specific spectral signatures associated with vegetation health and burn severity, enabling accurate detection and mapping of fire-affected areas. Utilizing Sentinel-2 spectral data enables the mapping of burned areas at a spatial resolution of 20 m and facilitates the identification of smaller burned areas [127].

The NBR is an index that combines the NIR and SWIR spectral bands, with theoretical values ranging between −1 and 1 [152]. This index is founded on the principle that burned areas exhibit an increase in reflectance in the SWIR band and a decrease in the NIR band. In the NIR band, reflectance diminishes due to the loss of leaves [153], whereas in the SWIR band, reflectance escalates as plant moisture content decreases [154,155]. Additionally, the NBR is sensitive to the contrast in reflectance between charred areas in the SWIR band and unburnt vegetation in the NIR band, as observed in the Sentinel-2 spectral bands.

2.5. Calculating Rao's Q Index

According to Rocchini et al. [156], Rao's Q is a quantitative metric employed to evaluate the similarity or dissimilarity between spatial patterns or distributions of ecological variables. The calculation of Rao's Q utilized a fixed window size of 9 × 9 pixels, which was chosen for the purpose of index retrieval [124]. The formula to calculate the Rao's Q Index was used according to Rocchini et al. [124,157] (Equation (1)):

$$Rao's\ Q = d_{ij} \times p_i \times p_j \quad (1)$$

In this context, d_{ij} denotes the spectral distance between pixel i and pixel j, whereas p_i represents the proportion of pixel i in relation to the total pixels within an $n \times n$ window, expressed as $p_i = \frac{1}{n^2}$.

The open-source repository created and developed for this research is called "Raoq_GEE" and can be accessed on GitHub 3.15.3 at the following URL: https://github.com/rafaelatiengo/Raoq_GEE (accessed on 3 January 2025). This repository contains methods implemented in Python, enabling users to replicate the research findings.

The delineation of the study area can be performed within the code by either specifying geographic coordinates or by directly drawing the polygon of interest on the map. This methodology offers considerable flexibility in data processing, accommodating a variety of use cases and strategies that prospective users may wish to employ. This adaptability increases the customizability of the code to suit a wide range of needs and specific applications, enhancing the system's overall versatility and utility. Additionally, users can incorporate shapefiles of the study area, provided they have the area saved in vector format on their devices, as previously outlined by [123,125].

The variation between each pair of Rao's Q maps is determined by the pixel values corresponding to the calculated change intensity [123], as described by Equation (2).

$$Root\ Square\ Difference = \sqrt{\left(Rao_{After} - Rao_{Before}\right)^2} \quad (2)$$

As shown in Figure 3, Rao's Q was calculated using both the classical mode and three multidimensional modes. While the classical Rao's Q approach is straightforward and facilitates interpretation, it may overlook complex interactions between indices, providing a limited perspective on LULCC. In contrast, the multidimensional approach enables a more comprehensive evaluation by integrating multiple spectral indices, thereby capturing interactions that can significantly enhance the detection of burned areas. In our study, the selected combinations for the multidimensional modes were MD 1 (NBR + MIRBI), MD 2 (NDVI + MIRBI), and MD 3 (NDVI + NBR). These combinations were selected based on their superior performance in the classical Rao's Q analysis, demonstrating optimal results in the detection of burned areas.

In this context, Rao's Q was calculated for wildfire scenarios. This study builds upon and extends the works of Tassi & Gil [122] and Tiengo et al. [125] by testing the approach to burnt areas incorporating fire-specific indices (MIRBI, BAIS2, NBR) and their combinations across three case studies with diverse climates and vegetation types. While Tassi & Gil [122] employed only NDVI and Landsat 8, and Tiengo et al. [125] focused on monitoring nature conservation areas using multiple sensors integrated with Google Earth Engine, our research differentiates itself by focusing on monitoring wildfires. Additionally, we tested and validated the use of Rao's Q for wildfire monitoring in areas with distinct environmental characteristics, thus expanding its application to new contexts that had not been explored in previous studies.

2.6. Threshold-Based Change Detection

The dissimilarity between each pair of Rao's Q maps, both pre-and post-event, is represented through pixel values that quantify the estimated change intensity. For each methodological approach (classic, MD 1, MD 2, and MD 3), a final binary map was produced, categorizing areas into "change" and "no change" classes based on a determined threshold.

The threshold used to classify areas as 'change' or 'no change' was determined using a histogram-based method. This approach involves analyzing the distribution of pixel values representing the intensity of changes observed in the difference maps between pre- and post-event Rao's Q Index. Specifically, the threshold is set by identifying the point of maximum perpendicular distance from the secant line that connects the histogram's highest and lowest points. This method effectively identifies an optimal cut-off point that separates significant changes from typical background variations [123,125].

2.7. Accuracy Assessment

To assess the accuracy of various Rao's Q-based methodologies in producing binary maps, we determined the OA as the percentage of accurate classifications. This procedure involved generating and evaluating 100 random points, created individually using QGIS 3.10, with 50 points marked as 'change' and 50 points marked as 'no change' for each case study. Each point's classification was verified and validated as accurate or inaccurate through GIS-based photo interpretation utilizing high-resolution orthophotomaps and satellite imagery (e.g., Google Earth), supported by the respective CEMS monitoring reports.

The criteria for classifying the values into these categories were based on the methods' accuracy classification, defined as follows: low agreement (below 40), moderate agreement

(41 to 60), good agreement (61 to 75), excellent agreement (76 to 80), and almost perfect agreement (above 80) [125,146,158–168].

Cohen's κ [169] was also used to check the level of agreement between producer and user accuracy. Although the κ-coefficient is a widely used metric, it is not without limitations. Therefore, accuracy was additionally assessed using the Allocation and Quantity Disagreement metrics (AD and QD, respectively [170], and by the True Skill Statistic (TSS; [163]). TSS ranges from −1 to +1, accounting for both omission (i.e., sensitivity) and commission (i.e., specificity) errors. According to Coetzee et al. [171]. TSS values below 0.5 are considered poor.

3. Results

3.1. Sardinia

On 13 July 2019, a wildfire ignited in the central-eastern region of the island of Sardinia, near the city of Tortolì, located in the Ogliastra province. The fire consumed approximately 800 hectares of Mediterranean shrublands [138]. Given the fire danger and the threatened values, the CEMS was activated on 17 July.

The study conducted on wildfire-affected areas in Sardinia provided valuable insights into the effectiveness of spectral indices for detecting burned areas using Rao's Q-based approaches. The individual indices using the classic Rao's Q approach were evaluated first, revealing varying levels of accuracy in identifying fire-impacted regions (Figure 4).

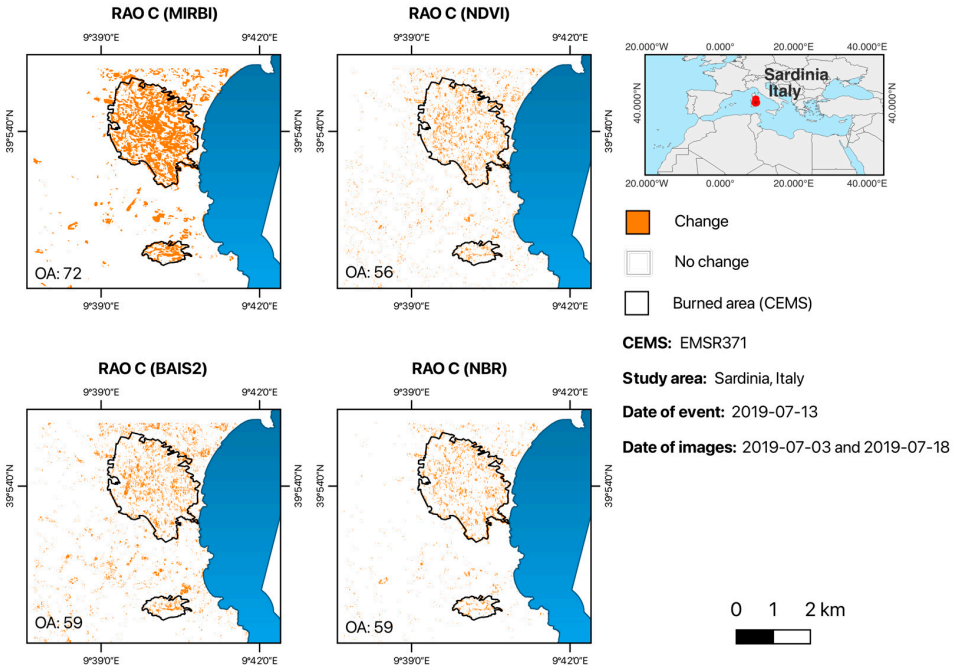

Figure 4. Accuracy assessment of Rao's Q classic on detecting burned areas in Sardinia: MIRBI performed best with an OA of 72%, followed by BAIS2 and NBR, both with 59%, and NDVI with 56%.

The MIRBI demonstrated the highest OA at 72%, followed by the BAIS2 and NBR, both with an OA of 59%. The NDVI recorded a lower OA of 56% (Table 4). However, these relatively low OA values are related to the identification of many false negatives, leading to overestimations in the burned area. In fact, the Specificity (s) values range from 55% (BAIS2 and NBR) to 66% (MIRBI). This imbalance in classification also explains the high values of Quantity Disagreement (QD) across all the spectral indices analyzed. The values of the κ coefficient and TSS are all below the thresholds required to consider the classification agreement as good (<0.60 and <0.75, respectively). However, while MIRBI shows the highest κ value (0.44), the highest TSS value was achieved by NBR (0.55).

Table 4. Accuracy metrics for each Rao's Q methodological approach (The values highlighted in bold represent OA, S, s and TSS greater than 0.75, κ greater than 0.60 and AD and QD less than 0.10).

			Accuracy Metrics						
Study Areas	**Approach**	**Spectral Metrics**	**OA**	**S**	**s**	**κ**	**TSS**	**AD**	**QD**
Sardinia (Italy)	Rao's Q Classic	MIRBI	0.72	**0.87**	0.66	0.44	0.52	**8.00**	20.00
		NDVI	0.56	**0.88**	0.53	0.12	0.41	**2.00**	42.00
		BAIS2	0.59	**0.85**	0.55	0.18	0.40	**4.00**	37.00
		NBR	0.59	**1.00**	0.55	0.18	0.55	**0.00**	41.00
	Rao's Q MD	MIRBI + NBR	**0.93**	**0.92**	**0.94**	**0.86**	**0.86**	**6.00**	**1.00**
		MIRBI + NDVI	**0.91**	**0.92**	**0.90**	**0.82**	**0.82**	**8.00**	**1.00**
		NBR + NDVI	0.73	**0.90**	0.66	0.46	0.56	**6.00**	21.00
Thassos (Greece)	Rao's Q Classic	MIRBI	0.56	**1.00**	0.53	0.12	0.53	**0.00**	44.00
		NDVI	0.67	**0.95**	0.60	0.34	0.55	**2.00**	31.00
		BAIS2	0.52	0.67	0.51	0.04	0.18	**4.00**	44.00
		NBR	0.63	**1.00**	0.57	0.26	0.57	**0.00**	37.00
	Rao's Q MD	MIRBI + NBR	**0.90**	**0.98**	**0.84**	**0.80**	**0.82**	2.00	**8.00**
		MIRBI + NDVI	**0.82**	**0.97**	0.74	**0.64**	0.71	**2.00**	16.00
		NBR + NDVI	**0.93**	**0.96**	**0.91**	**0.86**	**0.86**	**4.00**	**3.00**
Pantelleria (Italy)	Rao's Q Classic	MIRBI	0.71	**0.89**	0.64	0.42	0.53	**6.00**	23.00
		NDVI	0.68	**1.00**	0.61	0.36	0.61	**0.00**	32.00
		BAIS2	0.57	**0.89**	0.54	0.14	0.43	**2.00**	41.00
		NBR	0.70	**1.00**	0.63	0.40	0.63	**0.00**	30.00
	Rao's Q MD	MIRBI + NBR	**0.96**	**0.98**	**0.94**	**0.92**	**0.92**	**2.00**	**2.00**
		MIRBI + NDVI	**0.77**	**1.00**	0.68	0.54	0.68	**0.00**	23.00
		NBR + NDVI	**0.78**	**0.97**	0.70	0.56	0.67	**2.00**	20.00

OA: Overall accuracy; S: Sensitivity; s: Specificity; κ: Cohen's kappa; TSS: True Skill Statistic; AD: Allocation disagreement; QD: Quantity disagreement.

In a subsequent analysis, different combinations of indices were tested by applying Rao's Q multidimensional approach to enhance detection capabilities (Figure 5).

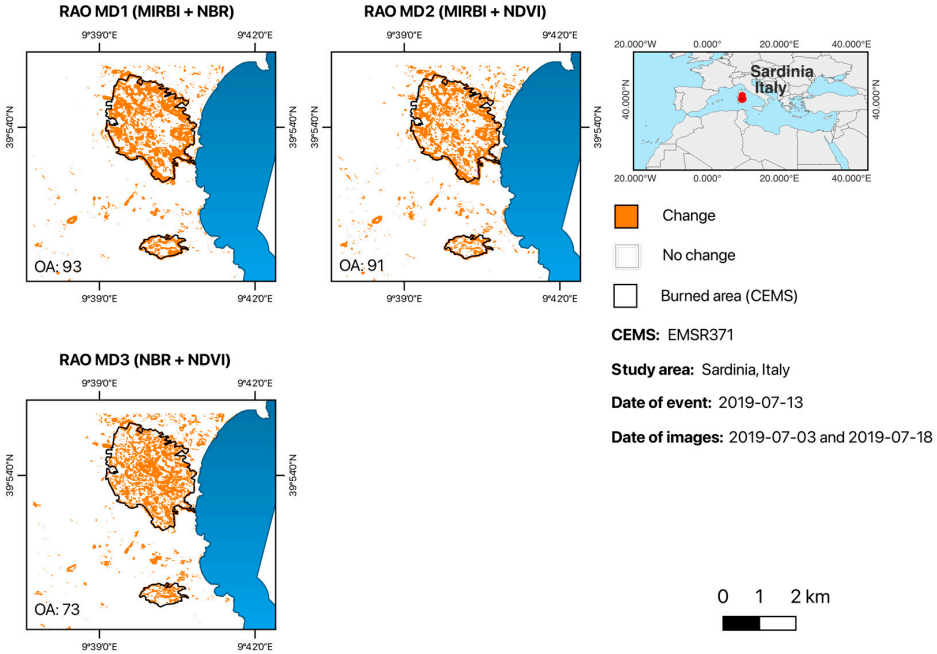

Figure 5. Effectiveness of Rao's Q MD in detecting burned areas in Sardinia: MIRBI + NBR achieved an OA of 93%, indicating superior detection capabilities. NBR + NDVI reached an OA of 73%, while MIRBI + NDVI had an OA of 91%, demonstrating the value of combining indices for more precise fire impact.

The MIRBI + NBR combination achieved a remarkably high OA of 93%, indicating superior performance in accurately delineating burned areas (Table 4). The MIRBI + NDVI combination yielded an OA of 91%, while the NBR + NDVI combination reached an OA of 73%. The values of the κ coefficient and TSS for the MIRBI + NBR and MIRBI + NDVI combinations indicate high levels of accuracy, highlighting their synergistic effect. These high values result from significant improvements in reducing false negatives, with clear effects on the QA metric (1% for both combinations). The NBR + NDVI combination outperforms the spectral indices in the classical approach but does not stand out from the performance of MIRBI. These results demonstrate that the OA for these combined indices was significantly higher, particularly for the MIRBI + NBR combination, highlighting the benefits of integrating multiple indices for more precise fire impact assessments.

3.2. Thassos

On 10 August, a wildfire ignited near the village of Potamia on Thassos Island, located in the Eastern Macedonia and Thrace Region of Greece. The fire burned through forest stands, shrubland, and agricultural areas [139]. In response to the disaster, the CEMS was activated on 17 August. The indices using the classic Rao's Q approach were first computed (Figure 6).

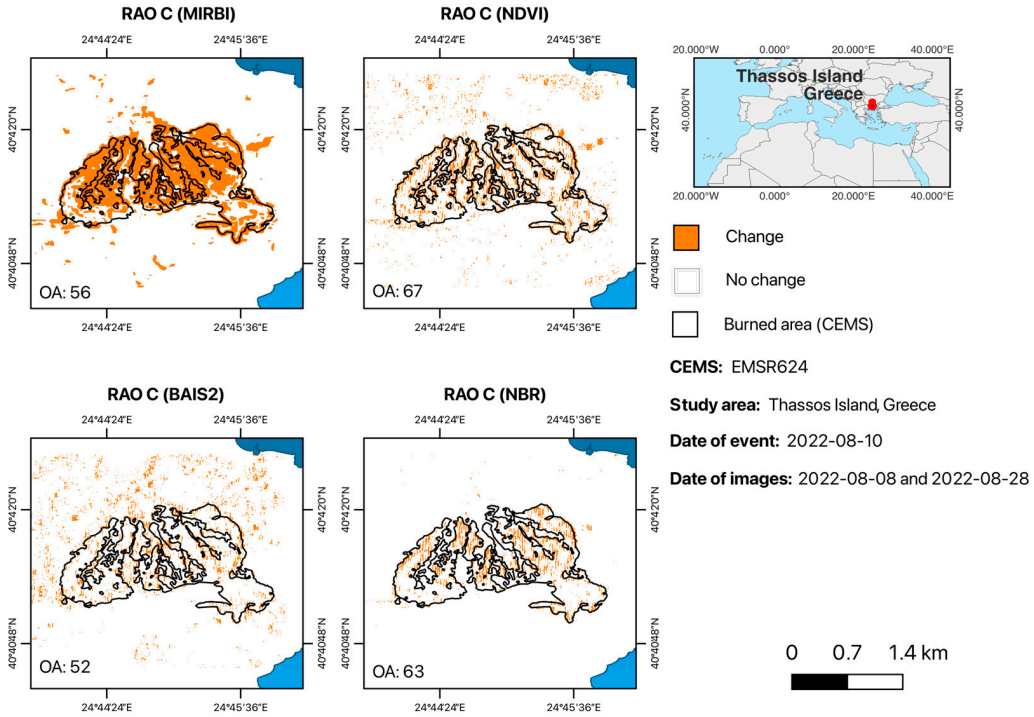

Figure 6. Effectiveness of Rao's Q classic for detecting burned areas in Thassos: NDVI exhibited the highest OA at 67%. NBR followed with an OA of 63, while MIRBI and BAIS2 demonstrated lower accuracy, with OAs of 56% and 52%, respectively.

NDVI achieved the highest OA of 67%, indicating a relatively strong performance in identifying fire-impacted areas (Table 4). The NBR followed with an OA of 63%, demonstrating moderate reliability. The MIRBI recorded an OA of 56%, while the BAIS2 had the lowest OA of 52%. However, both the κ coefficients and the TSS values are very low. The highest κ value was determined by the NDVI (0.34, fair agreement), and the highest TSS value with the NBR (0.57, moderate accuracy). The same issue identified in the previous case study is observed regarding the identification of false negatives, resulting in low values of the Specificity metric (between 0.51 and 0.60) and moderately high values of the Quantity Disagreement (QD between 31% and 44%).

Additional analysis involved testing the combination of the three top-performing individual spectral indices by applying Rao's Q multidimensional approach (Figure 7).

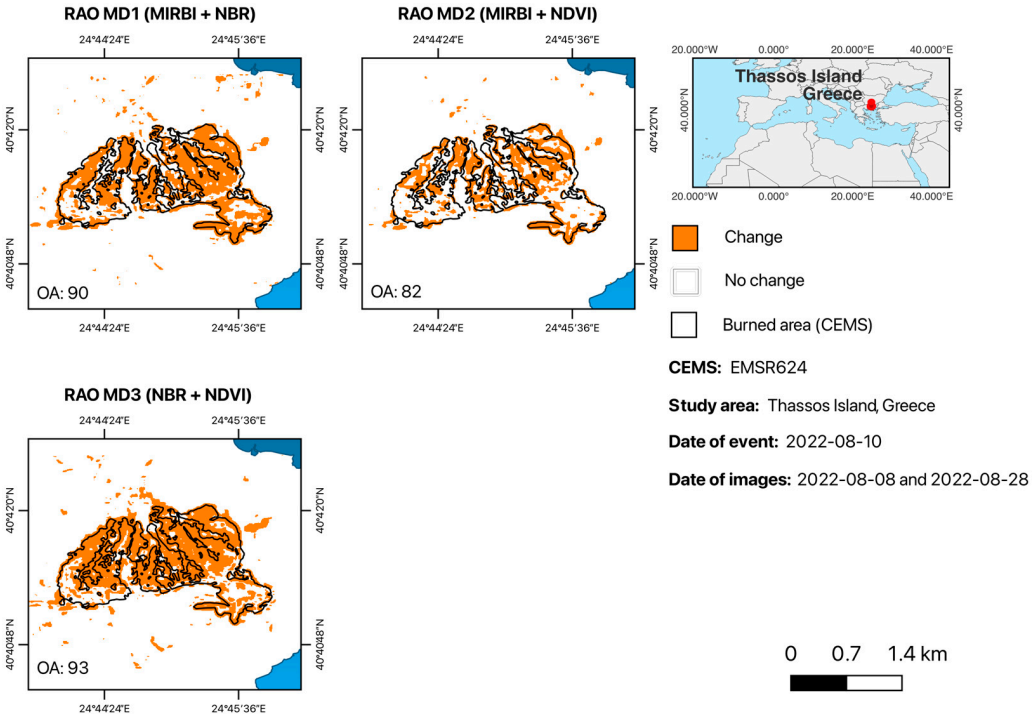

Figure 7. Effectiveness of Rao's Q MD for detecting burned areas in Thassos: the MIRBI + NBR combination achieved an OA of 90%. The combinations of MIRBI + NDVI showed an OA of 82% and the NBR + NDVI an OA of 93%, indicating its superior accuracy in mapping burned areas.

The MIRBI + NBR combination resulted in an exceptional OA of 90%, highlighting its superior ability to accurately delineate burned areas in this context (Table 4). The MIRBI + NDVI combination achieved an OA of 82%, and the NBR + NDVI combination yielded an OA of 93%, both showing significant improvements over the individual indices. The improvement in performance with these combinations is mainly due to the reduction of false negatives ($0.74 \leq s \leq 0.91$), with reflections in the QD metric ($3\% \leq QD \leq 16\%$). In this case study, the greatest synergetic effects appear to come from the use of the NBR index, reaching the highest values of κ and TSS when combined with NDVI (0.86 in both accuracy metrics). These results underscore the advantage of integrating multiple indices for more precise and reliable fire impact assessments in Thassos.

3.3. Pantelleria

On 17 August, a significant wildfire, sparked by two separate ignitions, erupted on the island of Pantelleria, Sicily, fueled by the strong Scirocco winds that continued to blow across the island [140]. In response, the CEMS was activated on 18 August. Rao's Q classic was computed for this event; its results are shown below (Figure 8).

Analyzing Rao's Q classic, MIRBI achieved an OA of 71%, indicating its effectiveness in identifying fire-impacted on this island (Table 4). The NBR closely followed with an OA of 70%, demonstrating comparable reliability. The NDVI showed an OA of 68%, while BAIS2 had the lowest accuracy among the classical indices, with an OA of 57%. The κ coefficient ranges from 0.14 (BAIS2) to 0.42 (MIRBI), and the TSS ranges from 0.43 (BAIS2) to 0.63 (NBR). In all cases, the performance of the indicators varies from low to moderate, again showing low values of Specificity ($0.54 \leq s \leq 0.64$) and moderately high values of Quantity Disagreement ($23\% \leq QD \leq 41\%$).

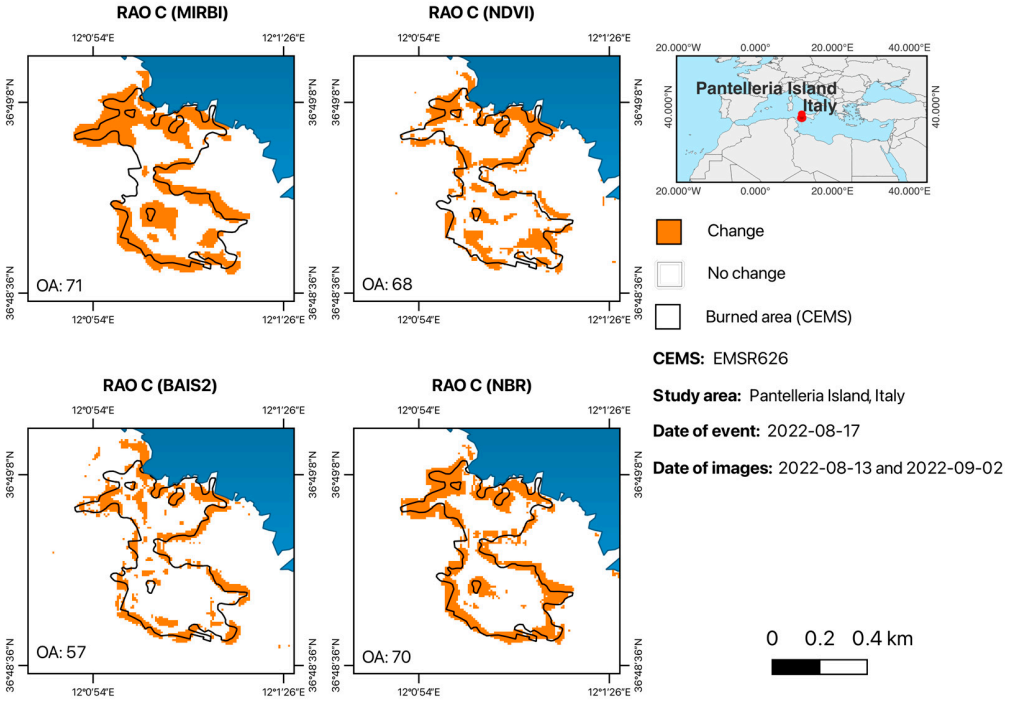

Figure 8. Effectiveness of Rao's Q classic for detecting burned areas in Thassos: MIRBI demonstrated the highest OA at 71%, followed closely by NBR with an OA of 70%. NDVI showed a moderate OA of 68%, while BAIS2 recorded the lowest OA of 57%, indicating a comparatively lower accuracy in identifying fire-impacted regions.

In subsequent evaluations, different sets of indices were utilized to enhance the capability for detection (Figure 9).

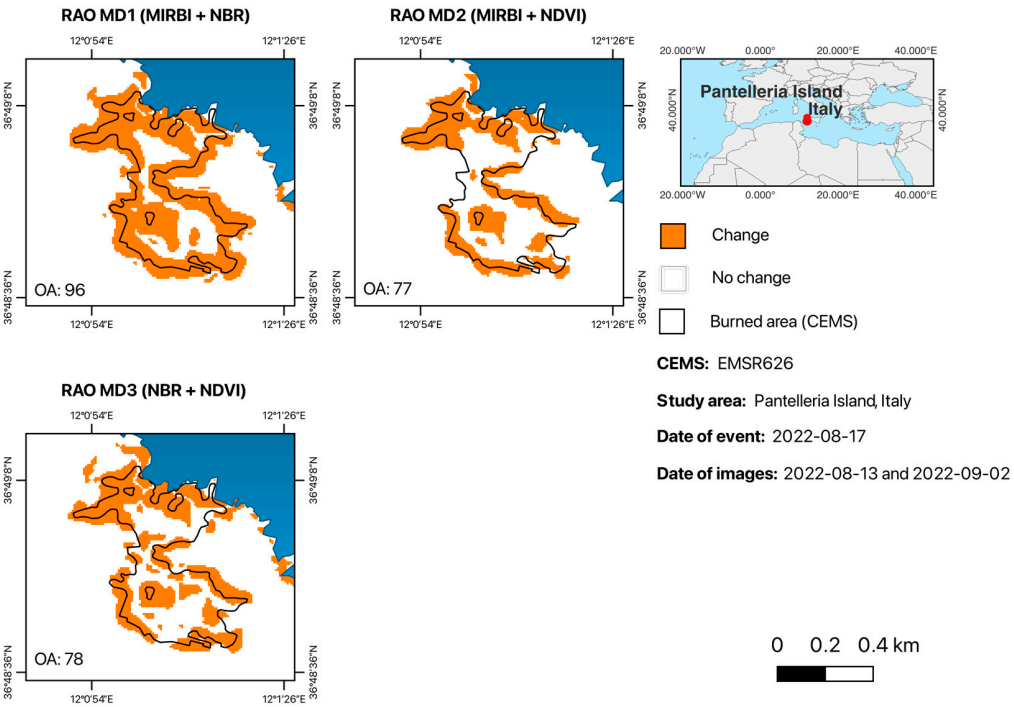

Figure 9. Effectiveness of Rao's Q MD for detecting burned areas in Pantelleria: the MIRBI + NBR combination achieved an exceptional OA of 96%, demonstrating superior accuracy in delineating burned areas. The MIRBI + NDVI and NBR + NDVI combinations also showed significant improvements, with OAs of 77% and 78%, respectively, highlighting the effectiveness of combining multiple indices for more precise fire impact assessments.

The combination of MIRBI + NBR achieved an outstanding OA of 96%, underscoring its superior performance in accurately delineating burned areas (Table 4). The NBR + NDVI combination recorded an OA of 78%, and the MIRBI + NDVI combination yielded an OA of 77%. However, from the analysis of the remaining accuracy metrics, it is observed that this synergistic effect is more relevant in the MIRBI + NBR combination, resulting in a κ coefficient and TSS of 0.92, Specificity of 94%, and Quantity Disagreement (QD) of only 2%. These results highlight the significant improvements in accuracy when integrating multiple indices, particularly the combination of MIRBI + NBR, for more precise fire impact assessments in Pantelleria.

3.4. Overall Accuracy Assessment

Table 4 presents the accuracy outcomes of the methodological approaches based on Rao's Q. Among these, Rao's Q MD employing the MIRBI and NBR index demonstrated better performance, highlighting its effectiveness in detecting LULCC resulting from wildfire events.

4. Discussion

This study evaluates the effectiveness of Rao's Q methodology in detecting burned areas across three distinct islands within the Mediterranean Basin: Sardinia, Thassos, and Pantelleria. The results highlight the usefulness of this methodology for detecting burned areas in the above locations. They also showed remarkable differences between spectral indices when used independently (classical approach) or in combination (multidimensional approach), which undoubtedly improved the results.

In the classical approach of the algorithm, the best results were obtained using the MIRBI (in Sardinia and Pantelleria) and the NDVI (in Thassos), while the worst results were obtained using the BAIS2 (in Thassos and Pantelleria) and the NDVI (in Sardinia), as shown in Table 4. These findings are consistent with previous studies that have demonstrated MIRBI's effectiveness in fire detection [141] due to its sensitivity to burnt vegetation and soil [172]. Several authors have noted its good performance, especially in arid savannahs, shrublands, and grasslands [173–175], which are the cover types for which this index was designed [109]. These ecosystems are characterised by a low canopy density, a consequent importance of the soil signal in the spectral response and a senescence that can often overlap with the arrival of the fire season. Additionally, Schepers et al. [173] found good performance of the MIRBI, especially in dry and highly flammable vegetation. Most of these characteristics are shared by the fire-affected ecosystems of Sardinia [150] and Panttelleria, which may explain the results achieved in these two study areas. However, whenever the vegetation cover is denser and more vigorous, as is more the case of Thassos, the spectral response after a fire is less evident in the mid-infrared spectrum (as captured by MIRBI) and more apparent in the red and NIR bands [131]. This same behavior has been shown by Fornaca et al. [175] demonstrating a better detection of burned areas when using indices that work with the NIR band, such as the NDVI or the NBR. The NDVI, by capturing the loss of green biomass and live fuel moisture, ensures good separability between burned and unburned areas in landscapes where vegetation is dense [146,151,152], which may explain the good results in Thassos, failing in regions with low primary productivity, such as Sardinia.

Despite the limitations shown by Roy et al. [145], the NBR index is one of the most widely used for mapping burned areas and severity [176–179]. In general, it tends to perform well in areas with dense, photosynthetically active vegetation [109,173], while it can misclassify bare soil, water bodies, or urban areas as burned. In fact, its performance can be influenced not only by vegetation density but also by the burn severity [109,151,180].

Additionally, effective detection was very robust over time when using this index, as shown by Schepers et al. [173] when analyzing coniferous forests. As shown in Table 4, the overall accuracy of this index under the classical approach reached the second highest value among the three study cases, demonstrating its ability to perform well in Mediterranean ecosystems of both low (Sardinia, Pantelleria) and medium vegetation density (Thassos). These favorable results could be attributed to the choice of images taken very close to the occurrence of the event, a crucial factor for the detection of burned areas in sparsely vegetated ecosystems [109].

The launch of the Sentinel-2 MSI series in 2015 opened up the possibility of calculating burned area spectral indices with improved spectral resolution, as is the case of BAIS2 [127]. This index benefits from either the first part of the red-edge region, where variations in chlorophyll content can be derived, the NIR part of the spectrum, more related to variation in leaf structure, or the SWIR bands, where burned area detection is known to be efficient [127]. The performance of BAIS2 and fourteen other indices in detecting burned areas was studied by van Dijk et al. [141]. Dijk et al. [141] concluded that the most effective Sentinel-2 bands for discriminating burned areas were the NIR and long red-edge wavelengths (bands 6, 7, and 8A) due to the decrease in the amount of vegetation after the fire. Also, the LSWIR band (band 12) showed a high discriminatory ability attributed to the change in the water content of the plant tissue. In terms of indices, those with the highest discriminating power were the ones using the two SWIR bands (bands 11 and 12). Despite the BAIS2 being a promising index [180], the results for the three areas studied for this index showed the lowest overall accuracy values in Thassos and Pantelleria and the second lowest in Sardinia (tied with the NBR) (see Table 4). Han et al. [180] have shown that this index is influenced by vegetation density and fire severity. Unfortunately, there is still little literature on this index to help us interpret these results. The low OA values for the BAIS2 index meant that it was discarded for the second stage of the algorithm, so Rao's Q MD was not calculated using the BAIS2 due to its consistently inferior performance in the classical Rao's Q analysis across all study areas.

In the multidimensional (MD) approach of the algorithm, the best results were obtained in all cases by combining the MIRBI and NBR indices. These results emphasize the value of combining indices to overcome the limitations of individual methods and improve the overall accuracy of fire performance assessment. These results are in line with those shown by other authors on the suitability of the MIRBI and NBR indices for the detection of burnt areas [141,175], especially in environments such as the Mediterranean basin. Other works have also shown the usefulness of combining several indices and using them synergistically in the assessment of the burnt area [181], highlighting the importance of integrating indices that can respond to the different responses of the land cover to the fire phenomenon.

In this study, the boundaries of burned areas were delineated using data provided by the CEMS. The results obtained from applying Rao's Q metric to detect burned areas were found to be consistent with the CEMS-provided delineations. This alignment validates the effectiveness of the employed indices and methods, as the CEMS data represents a reliable and authoritative source for assessing fire-affected regions. The concurrence between the detected burned areas and CEMS boundaries reinforces the accuracy of our results and supports the robustness of our validation approach. By aligning our findings with established CEMS limits, we ensure that our analysis provides a credible and comparable assessment of fire impacts, thereby enhancing the reliability and applicability of our results in fire management and response efforts.

5. Conclusions

This study provides a comprehensive evaluation of the effectiveness of various indices in detecting burned areas across Sardinia, Thassos, and Pantelleria using Rao's Q. The analysis demonstrates that while individual classical indices such as MIRBI, NBR, and NDVI exhibit varying levels of accuracy in identifying fire-impacted regions, combining these indices enhance significantly detection capabilities. The multidimensional approach leverages the strengths of individual indices and Sentinel-2 MSI's improved spectral resolution, particularly in the SWIR and NIR bands. This advancement is crucial for accurate burned area delineation in diverse Mediterranean ecosystems. Integrating indices with complementary spectral sensitivities provides a robust tool for fire prevention strategies, resource allocation, and ecological restoration planning.

Overall, the results from Sardinia, Thassos, and Pantelleria illustrate the variability in index performance and the advantages of combining multiple indices to enhance detection accuracy. The study underscores the importance of selecting appropriate indices and combinations based on regional characteristics and specific detection needs. Future research should continue to explore and validate these approaches across diverse landscapes to refine wildfire detection methodologies further and improve overall wildfire management strategies.

The findings affirm that integrating multiple indices, particularly MIRBI and NBR, provides a robust approach to enhancing fire detection accuracy. This synergistic approach improves accuracy and highlights the value of incorporating spectral responses to fire phenomena. The boundaries of burned areas were detected using Rao's Q metric, which was aligned with those provided by the Copernicus Emergency Management Service (CEMS). This consistency validates the reliability and robustness of the fire detection and assessment methodology. It facilitates its adoption by policymakers, land managers, and emergency response teams for reliable fire impact assessments.

This study introduces a novel methodology for detecting and mapping burned areas by adapting Rao's Q index—traditionally used to measure spatial heterogeneity—to wildfire monitoring. Using high-resolution Sentinel-2 imagery, the approach integrates multiple spectral indices, namely NDVI, NBR, MIRBI, and BAIS2, individually and in a multidimensional framework. Notably, the multidimensional method significantly enhances detection accuracy, demonstrating that the multidimensional approach may overcome the limitations inherent in single-index methods, such as false negatives and commission errors. Validation against authoritative Copernicus Emergency Management Service (CEMS) data confirms the robustness of the results. This work also provides an open-source, reproducible workflow using Python integrated with Google Earth Engine, facilitating further application and development. It pioneers the application of Rao's Q index in burned area detection and sets a new and robust approach for utilizing freely accessible remote sensing data in fire monitoring and management.

Author Contributions: Conceptualization, R.T. and A.G.; methodology, R.T., N.G., J.U. and A.G.; code, R.T. and J.U.; validation, R.T. and J.U.; data curation, R.T. and J.U.; writing—original draft preparation, R.T.; writing—review and editing, N.G., A.G. and S.M.-D.-M.; supervision, A.G. and S.M.-D.-M. All authors have read and agreed to the published version of the manuscript.

Funding: Nuno Guiomar was funded by the European Union through the European Regional Development Fund in the framework of the Interreg V-A Spain-Portugal program (POCTEP) under the FIREPOCTEP+ (Ref. FIREPOCTEP+ (0139_FIREPOCTEP_MAS_6_E)) project and by National Funds through FCT under the projects MED UIDB/05183 and CHANGE LA/P/0121/2020 (DOI 10.54499/LA/P/0121/2020). Artur Gil's contribution was supported by the IVAR grant from Fundação para a Ciência e Tecnologia ref. UIDP/00643/2020 (DOI: https://doi.org/10.54499/UIDP/00643/2020).

Data Availability Statement: The open-source repository created and developed for this research was named "Raoq_GEE" and is accessible on GitHub at https://github.com/rafaelatiengo/Raoq_GEE (accessed on 3 January 2025). Users can locate the Python-implemented methods within the repository to reproduce the research results.

Acknowledgments: The authors gratefully acknowledge Andrea Tassi for developing and freely providing in his GitHub repository (https://github.com/AndreaTassi23/spectralrao-monitoring (accessed on 15 July 2024)) the Rao's Q-based agricultural LULCC detection operational framework and for the additional information and materials shared.

Conflicts of Interest: The authors declare no conflicts of interest. The funders had no role in the study's design; in the collection, analyses, or interpretation of the data; in the writing of the manuscript; or in the decision to publish the results.

References

1. Bowman, D.M.J.S.; Balch, J.K.; Artaxo, P.; Bond, W.J.; Carlson, J.M.; Cochrane, M.A.; D'Antonio, C.M.; DeFries, R.S.; Doyle, J.C.; Harrison, S.P.; et al. Fire in the Earth System. *Science* **2009**, *324*, 481–484. [CrossRef] [PubMed]
2. McLauchlan, K.K.; Higuera, P.E.; Miesel, J.; Rogers, B.M.; Schweitzer, J.; Shuman, J.K.; Tepley, A.J.; Varner, J.M.; Veblen, T.T.; Adalsteinsson, S.A.; et al. Fire as a Fundamental Ecological Process: Research Advances and Frontiers. *J. Ecol.* **2020**, *108*, 2047–2069. [CrossRef]
3. Bond, W.J.; Woodward, F.I.; Midgley, G.F. The Global Distribution of Ecosystems in a World without Fire. *New Phytol.* **2005**, *165*, 525–538. [CrossRef]
4. Bond, W.; Keeley, J. Fire as a Global 'Herbivore': The Ecology and Evolution of Flammable Ecosystems. *Trends Ecol. Evol.* **2005**, *20*, 387–394. [CrossRef]
5. Pausas, J.G.; Verdú, M. Fire reduces morphospace occupation in plant communities. *Ecology* **2008**, *89*, 2181–2186. [CrossRef]
6. Dantas, V.d.L.; Pausas, J.G.; Batalha, M.A.; Paula Loiola, P.d.; Cianciaruso, M.V. The Role of Fire in Structuring Trait Variability in Neotropical Savannas. *Oecologia* **2013**, *171*, 487–494. [CrossRef]
7. Pausas, J.G.; Keeley, J.E. Evolutionary Ecology of Resprouting and Seeding in Fire-prone Ecosystems. *New Phytol.* **2014**, *204*, 55–65. [CrossRef] [PubMed]
8. Pausas, J.G.; Ribeiro, E. Fire and Plant Diversity at the Global Scale. *Glob. Ecol. Biogeogr.* **2017**, *26*, 889–897. [CrossRef]
9. He, T.; Lamont, B.B. Fire as a Potent Mutagenic Agent Among Plants. *CRC Crit. Rev. Plant Sci.* **2018**, *37*, 1–14. [CrossRef]
10. Lamont, B.B. Historical Links between Climate and Fire on Species Dispersion and Trait Evolution. *Plant Ecol.* **2022**, *223*, 711–732. [CrossRef]
11. Countryman, C. *The Fire Environment Concept*; Pacific Southwest Forest and Range Experiment Station: Berkeley, CA, USA, 1972.
12. Krawchuk, M.A.; Moritz, M.A.; Parisien, M.-A.; Van Dorn, J.; Hayhoe, K. Global Pyrogeography: The Current and Future Distribution of Wildfire. *PLoS ONE* **2009**, *4*, e5102. [CrossRef]
13. Murphy, B.P.; Bradstock, R.A.; Boer, M.M.; Carter, J.; Cary, G.J.; Cochrane, M.A.; Fensham, R.J.; Russell-Smith, J.; Williamson, G.J.; Bowman, D.M.J.S. Fire Regimes of Australia: A Pyrogeographic Model System. *J. Biogeogr.* **2013**, *40*, 1048–1058. [CrossRef]
14. Pausas, J.G. Pyrogeography across the Western Palaearctic: A Diversity of Fire Regimes. *Glob. Ecol. Biogeogr.* **2022**, *31*, 1923–1932. [CrossRef]
15. Cunningham, C.X.; Williamson, G.J.; Nolan, R.H.; Teckentrup, L.; Boer, M.M.; Bowman, D.M.J.S. Pyrogeography in Flux: Reorganization of Australian Fire Regimes in a Hotter World. *Glob. Change Biol.* **2024**, *30*, e17130. [CrossRef]
16. El Garroussi, S.; Di Giuseppe, F.; Barnard, C.; Wetterhall, F. Europe Faces up to Tenfold Increase in Extreme Fires in a Warming Climate. *npj Clim. Atmos. Sci.* **2024**, *7*, 30. [CrossRef]
17. Andela, N.; Morton, D.C.; Giglio, L.; Chen, Y.; van der Werf, G.R.; Kasibhatla, P.S.; DeFries, R.S.; Collatz, G.J.; Hantson, S.; Kloster, S.; et al. A Human-Driven Decline in Global Burned area. *Science* **2017**, *356*, 1356–1362. [CrossRef]
18. Correa, D.B.; Alcântara, E.; Libonati, R.; Massi, K.G.; Park, E. Increased Burned area in the Pantanal over the Past Two Decades. *Sci. Total Environ.* **2022**, *835*, 155386. [CrossRef] [PubMed]
19. Cunningham, C.X.; Williamson, G.J.; Bowman, D.M.J.S. Increasing Frequency and Intensity of the Most Extreme Wildfires on Earth. *Nat. Ecol. Evol.* **2024**, *8*, 1420–1425. [CrossRef] [PubMed]
20. Collins, L.; Clarke, H.; Clarke, M.F.; McColl Gausden, S.C.; Nolan, R.H.; Penman, T.; Bradstock, R. Warmer and Drier Conditions Have Increased the Potential for Large and Severe Fire Seasons across South-eastern Australia. *Glob. Ecol. Biogeogr.* **2022**, *31*, 1933–1948. [CrossRef]

21. Boulanger, Y.; Arseneault, D.; Bélisle, A.C.; Bergeron, Y.; Boucher, J.; Boucher, Y.; Waldron, K. The 2023 Wildfire Season in Québec: An Overview of Extreme Conditions, Impacts, Lessons Learned and Considerations for the Future. *Can. J. For. Res.* **2024**, *55*. [CrossRef]
22. Zong, X.; Tian, X.; Yao, Q.; Brown, P.M. An Analysis of Fatalities from Forest Fires in China, 1951–2018. *Int. J. Wildland Fire* **2022**, *31*, 507–517. [CrossRef]
23. Molina-Terrén, D.M.; Xanthopoulos, G.; Diakakis, M.; Ribeiro, L.; Caballero, D.; Delogu, G.M.; Viegas, D.X.; Silva, C.A.; Cardil, A. Analysis of Forest Fire Fatalities in Southern Europe: Spain, Portugal, Greece and Sardinia (Italy). *Int. J. Wildland Fire* **2019**, *28*, 85. [CrossRef]
24. Ribeiro, L.M.; Rodrigues, A.; Lucas, D.; Viegas, D.X. The Impact on Structures of the Pedrógão Grande Fire Complex in June 2017 (Portugal). *Fire* **2020**, *3*, 57. [CrossRef]
25. Higuera, P.E.; Cook, M.C.; Balch, J.K.; Stavros, E.N.; Mahood, A.L.; St. Denis, L.A. Shifting Social-Ecological Fire Regimes Explain Increasing Structure Loss from Western Wildfires. *PNAS Nexus* **2023**, *2*. [CrossRef]
26. Guiomar, N.; Godinho, S.; Fernandes, P.M.; Machado, R.; Neves, N.; Fernandes, J.P. Wildfire Patterns and Landscape Changes in Mediterranean Oak Woodlands. *Sci. Total Environ.* **2015**, *536*, 338–352. [CrossRef]
27. Roy, D.P.; De Lemos, H.; Huang, H.; Giglio, L.; Houborg, R.; Miura, T. Multi-Resolution Monitoring of the 2023 Maui Wildfires, Implications and Needs for Satellite-Based Wildfire Disaster Monitoring. *Sci. Remote Sens.* **2024**, *10*, 100142. [CrossRef]
28. Xanthopoulos, G.; Athanasiou, M. Attica Region, Greece July 2018: A Tale of Two Fires and a Seaside Tragedy. *Wildifre* **2019**, *28*, 18–21.
29. Lagouvardos, K.; Kotroni, V.; Giannaros, T.M.; Dafis, S. Meteorological Conditions Conducive to the Rapid Spread of the Deadly Wildfire in Eastern Attica, Greece. *Bull. Am. Meteorol. Soc.* **2019**, *100*, 2137–2145. [CrossRef]
30. Viegas, D.X.; Stipanicev, D.; Ribeiro, L.; Pita, L.P.; Rossa, C. The Kornati Fire Accident—Eruptive Fire in Relatively Low Fuel Load Herbaceous Fuel Conditions. *WIT Trans. Ecol. Environ.* **2008**, *119*, 365–375.
31. Xanthopoulos, G.; Galloway, A. An International Perspective on Fatal Wildfires. In *The Path of Flames*; CRC Press: Boca Raton, FL, USA, 2023; pp. 1–24.
32. Couto, F.T.; Salgado, R.; Guiomar, N. Forest Fires in Madeira Island and the Fire Weather Created by Orographic Effects. *Atmosphere* **2021**, *12*, 827. [CrossRef]
33. Filipponi, F. Exploitation of Sentinel-2 Time Series to Map Burned areas at the National Level: A Case Study on the 2017 Italy Wildfires. *Remote Sens.* **2019**, *11*, 622. [CrossRef]
34. Malandra, F.; Vitali, A.; Morresi, D.; Garbarino, M.; Foster, D.E.; Stephens, S.L.; Urbinati, C. Burn Severity Drivers in Italian Large Wildfires. *Fire* **2022**, *5*, 180. [CrossRef]
35. Badeau, J.; Guibal, F.; Fulé, P.Z.; Chauchard, S.; Moneglia, P.; Carcaillet, C. 202 Years of Changes in Mediterranean Fire Regime in Pinus Nigra Forest, Corsica. *For. Ecol. Manag.* **2024**, *554*, 121658. [CrossRef]
36. Molina-Terrén, D.M.; Fry, D.L.; Grillo, F.F.; Cardil, A.; Stephens, S.L. Fire History and Management of Pinuscanariensis Forests on the Western Canary Islands Archipelago, Spain. *For. Ecol. Manag.* **2016**, *382*, 184–192. [CrossRef]
37. Collins, R.D.; de Neufville, R.; Claro, J.; Oliveira, T.; Pacheco, A.P. Forest Fire Management to Avoid Unintended Consequences: A Case Study of Portugal Using System Dynamics. *J. Environ. Manag.* **2013**, *130*, 1–9. [CrossRef] [PubMed]
38. Ingalsbee, T. Whither the Paradigm Shift? Large Wildland Fires and the Wildfire Paradox Offer Opportunities for a New Paradigm of Ecological Fire Management. *Int. J. Wildland Fire* **2017**, *26*, 557. [CrossRef]
39. Castellnou, M.; Prat-Guitart, N.; Arilla, E.; Larrañaga, A.; Nebot, E.; Castellarnau, X.; Vendrell, J.; Pallàs, J.; Herrera, J.; Monturiol, M.; et al. Empowering Strategic Decision-Making for Wildfire Management: Avoiding the Fear Trap and Creating a Resilient Landscape. *Fire Ecol.* **2019**, *15*, 31. [CrossRef]
40. Xanthopoulos, G.; Leone, V.; Delogu, G.M. The Suppression Model Fragilities. In *Extreme Wildfire Events and Disasters*; Elsevier: Amsterdam, The Netherlands, 2020; pp. 135–153.
41. Moreira, F.; Ascoli, D.; Safford, H.; Adams, M.A.; Moreno, J.M.; Pereira, J.M.C.; Catry, F.X.; Armesto, J.; Bond, W.; González, M.E.; et al. Wildfire Management in Mediterranean-Type Regions: Paradigm Change Needed. *Environ. Res. Lett.* **2020**, *15*, 011001. [CrossRef]
42. Rego, F.; Fernandes, P.; Rigolot, E. *Towards Integrated Fire Management: Outcomes of the European Project Fire Paradox*; European Forest Institute: Joensuu, Finland, 2010; Volume 23.
43. Moore, P.F. Global Wildland Fire Management Research Needs. *Curr. For. Rep.* **2019**, *5*, 210–225. [CrossRef]
44. Fernandes, P.M. Fire-Smart Management of Forest Landscapes in the Mediterranean Basin under Global Change. *Landsc. Urban Plan.* **2013**, *110*, 175–182. [CrossRef]
45. Tedim, F.; Leone, V.; Xanthopoulos, G. A Wildfire Risk Management Concept Based on a Social-Ecological Approach in the European Union: Fire Smart Territory. *Int. J. Disaster Risk Reduct.* **2016**, *18*, 138–153. [CrossRef]

46. Pais, S.; Aquilué, N.; Campos, J.; Sil, Â.; Marcos, B.; Martínez-Freiría, F.; Domínguez, J.; Brotons, L.; Honrado, J.P.; Regos, A. Mountain Farmland Protection and Fire-Smart Management Jointly Reduce Fire Hazard and Enhance Biodiversity and Carbon Sequestration. *Ecosyst. Serv.* **2020**, *44*, 101143. [CrossRef]
47. Ascoli, D.; Plana, E.; Oggioni, S.D.; Tomao, A.; Colonico, M.; Corona, P.; Giannino, F.; Moreno, M.; Xanthopoulos, G.; Kaoukis, K.; et al. Fire-Smart Solutions for Sustainable Wildfire Risk Prevention: Bottom-up Initiatives Meet Top-down Policies under EU Green Deal. *Int. J. Disaster Risk Reduct.* **2023**, *92*, 103715. [CrossRef]
48. Guiomar, N.G.; Pereira, J.M.C.; Fernandes, P.M. A Planning Model for Fire-Resilient Landscapes in Portugal Is Riddled with Fallacies: A Critical Review of "FIRELAN" by Magalhães et al., 2021. *Fire* **2023**, *6*, 398. [CrossRef]
49. Pulido, F.; Corbacho, J.; Bertomeu, M.; Gómez, Á.; Guiomar, N.; Juárez, E.; Lucas, B.; Moreno, G.; Navalpotro, J.; Palomo, G. Fire-Smart Territories: A Proof of Concept Based on Mosaico Approach. *Landsc. Ecol.* **2023**, *38*, 3353–3370. [CrossRef]
50. Regos, A.; Pais, S.; Campos, J.C.; Lecina-Diaz, J. Nature-Based Solutions to Wildfires in Rural Landscapes of Southern Europe: Let's Be Fire-Smart! *Int. J. Wildland Fire* **2023**, *32*, 942–950. [CrossRef]
51. Benali, A.; Guiomar, N.; Gonçalves, H.; Mota, B.; Silva, F.; Fernandes, P.M.; Mota, C.; Penha, A.; Santos, J.; Pereira, J.M.C.; et al. The Portuguese Large Wildfire Spread Database (PT-FireSprd). *Earth Syst. Sci. Data* **2023**, *15*, 3791–3818. [CrossRef]
52. Davim, D.A.; Rossa, C.G.; Pereira, J.M.C.; Guiomar, N.; Fernandes, P.M. The Effectiveness of Past Wildfire at Limiting Reburning Is Short-Lived in a Mediterranean Humid Climate. *Fire Ecol.* **2023**, *19*, 66. [CrossRef]
53. Chuvieco, E.; Aguado, I.; Salas, J.; García, M.; Yebra, M.; Oliva, P. Satellite Remote Sensing Contributions to Wildland Fire Science and Management. *Curr. For. Rep.* **2020**, *6*, 81–96. [CrossRef]
54. Meng, R.; Zhao, F. Remote Sensing of Fire Effects: A Review for Recent Advances in Burned area and Burn Severity Mapping. In *Remote Sensing of Hydrometeorological Hazards*; Taylor & Francis Group: Boca Raton, FL, USA, 2017; pp. 261–283.
55. Nelson, D.M.; He, Y.; Moore, G.W.K. Trends and Applications in Wildfire Burned area Mapping: Remote Sensing Data, Cloud Geoprocessing Platforms, and Emerging Algorithms Author Links Open Overlay Panel. *Geomatica* **2024**, *76*, 100008. [CrossRef]
56. Chuvieco, E.; Yue, C.; Heil, A.; Mouillot, F.; Alonso-Canas, I.; Padilla, M.; Pereira, J.M.; Oom, D.; Tansey, K. A New Global Burned area Product for Climate Assessment of Fire Impacts. *Glob. Ecol. Biogeogr.* **2016**, *25*, 619–629. [CrossRef]
57. Alonso-Canas, I.; Chuvieco, E. Global Burned area Mapping from ENVISAT-MERIS and MODIS Active Fire Data. *Remote Sens. Environ.* **2015**, *163*, 140–152. [CrossRef]
58. Giglio, L.; Boschetti, L.; Roy, D.P.; Humber, M.L.; Justice, C.O. The Collection 6 MODIS Burned area Mapping Algorithm and Product. *Remote Sens. Environ.* **2018**, *217*, 72–85. [CrossRef] [PubMed]
59. Giglio, L.; Loboda, T.; Roy, D.P.; Quayle, B.; Justice, C.O. An Active-Fire Based Burned area Mapping Algorithm for the MODIS Sensor. *Remote Sens. Environ.* **2009**, *113*, 408–420. [CrossRef]
60. Roy, D.P.; Boschetti, L.; Justice, C.O.; Ju, J. The Collection 5 MODIS Burned area Product—Global Evaluation by Comparison with the MODIS Active Fire Product. *Remote Sens. Environ.* **2008**, *112*, 3690–3707. [CrossRef]
61. Plummer, S.; Arino, O.; Simon, M.; Steffen, W. Establishing A Earth Observation Product Service For The Terrestrial Carbon Community: The Globcarbon Initiative. *Mitig. Adapt. Strateg. Glob. Change* **2006**, *11*, 97–111. [CrossRef]
62. Tansey, K.; Grégoire, J.; Defourny, P.; Leigh, R.; Pekel, J.; van Bogaert, E.; Bartholomé, E. A New, Global, Multi-annual (2000–2007) Burned area Product at 1 Km Resolution. *Geophys. Res. Lett.* **2008**, *35*, 1–6. [CrossRef]
63. Tansey, K.; Grégoire, J.; Stroppiana, D.; Sousa, A.; Silva, J.; Pereira, J.M.C.; Boschetti, L.; Maggi, M.; Brivio, P.A.; Fraser, R.; et al. Vegetation Burning in the Year 2000: Global Burned area Estimates from SPOT VEGETATION Data. *J. Geophys. Res. Atmos.* **2004**, *109*. [CrossRef]
64. Murphy, B.P.; Russell-Smith, J. Fire Severity in a Northern Australian Savanna Landscape: The Importance of Time since Previous Fire. *Int. J. Wildland Fire* **2010**, *19*, 46. [CrossRef]
65. Andela, N.; Morton, D.C.; Giglio, L.; Paugam, R.; Chen, Y.; Hantson, S.; van der Werf, G.R.; Randerson, J.T. The Global Fire Atlas of Individual Fire Size, Duration, Speed and Direction. *Earth Syst. Sci. Data* **2019**, *11*, 529–552. [CrossRef]
66. Boschetti, L.; Roy, D.P.; Giglio, L.; Huang, H.; Zubkova, M.; Humber, M.L. Global Validation of the Collection 6 MODIS Burned area Product. *Remote Sens. Environ.* **2019**, *235*, 111490. [CrossRef]
67. Padilla, M.; Stehman, S.V.; Ramo, R.; Corti, D.; Hantson, S.; Oliva, P.; Alonso-Canas, I.; Bradley, A.V.; Tansey, K.; Mota, B.; et al. Comparing the Accuracies of Remote Sensing Global Burned area Products Using Stratified Random Sampling and Estimation. *Remote Sens. Environ.* **2015**, *160*, 114–121. [CrossRef]
68. Mouillot, F.; Schultz, M.G.; Yue, C.; Cadule, P.; Tansey, K.; Ciais, P.; Chuvieco, E. Ten Years of Global Burned area Products from Spaceborne Remote Sensing—A Review: Analysis of User Needs and Recommendations for Future Developments. *Int. J. Appl. Earth Obs. Geoinf.* **2014**, *26*, 64–79. [CrossRef]
69. Randerson, J.T.; Chen, Y.; van der Werf, G.R.; Rogers, B.M.; Morton, D.C. Global Burned area and Biomass Burning Emissions from Small Fires. *J. Geophys. Res Biogeosci.* **2012**, *117*, 1–23. [CrossRef]
70. Silva, J.M.N.; Sá, A.C.L.; Pereira, J.M.C. Comparison of Burned area Estimates Derived from SPOT-VEGETATION and Landsat ETM+ Data in Africa: Influence of Spatial Pattern and Vegetation Type. *Remote Sens. Environ.* **2005**, *96*, 188–201. [CrossRef]

71. Laris, P.S. Spatiotemporal Problems with Detecting and Mapping Mosaic Fire Regimes with Coarse-Resolution Satellite Data in Savanna Environments. *Remote Sens. Environ.* **2005**, *99*, 412–424. [CrossRef]
72. Roteta, E.; Bastarrika, A.; Padilla, M.; Storm, T.; Chuvieco, E. Development of a Sentinel-2 Burned area Algorithm: Generation of a Small Fire Database for Sub-Saharan Africa. *Remote Sens. Environ.* **2019**, *222*, 1–17. [CrossRef]
73. Oliveira, E.; Fernandes, P.M.; Barros, D.; Guiomar, N. Unraveling the Effect of Fire Seasonality on Fire-Preferred Fuel Types and Dynamics in Alto Minho, Portugal (2000–2018). *Fire* **2023**, *6*, 267. [CrossRef]
74. van der Werf, G.R.; Randerson, J.T.; Giglio, L.; van Leeuwen, T.T.; Chen, Y.; Rogers, B.M.; Mu, M.; van Marle, M.J.E.; Morton, D.C.; Collatz, G.J.; et al. Global Fire Emissions Estimates during 1997–2016. *Earth Syst. Sci. Data* **2017**, *9*, 697–720. [CrossRef]
75. Van Der Werf, G.R.; Randerson, J.T.; Giglio, L.; Collatz, G.J.; Mu, M.; Kasibhatla, P.S.; Morton, D.C.; Defries, R.S.; Jin, Y.; Van Leeuwen, T.T. Global Fire Emissions and the Contribution of Deforestation, Savanna, Forest, Agricultural, and Peat Fires (1997–2009). *Atmos. Chem. Phys.* **2010**, *10*, 11707–11735. [CrossRef]
76. Scholes, R.J.; Kendall, J.; Justice, C.O. The Quantity of Biomass Burned in Southern Africa. *J. Geophys. Res. Atmos.* **1996**, *101*, 23667–23676. [CrossRef]
77. Bastarrika, A.; Chuvieco, E.; Martín, M.P. Mapping Burned areas from Landsat TM/ETM+ Data with a Two-Phase Algorithm: Balancing Omission and Commission Errors. *Remote Sens. Environ.* **2011**, *115*, 1003–1012. [CrossRef]
78. Goodwin, N.R.; Collett, L.J. Development of an Automated Method for Mapping Fire History Captured in Landsat TM and ETM + Time Series across Queensland, Australia. *Remote Sens. Environ.* **2014**, *148*, 206–221. [CrossRef]
79. Hawbaker, T.J.; Vanderhoof, M.K.; Beal, Y.-J.; Takacs, J.D.; Schmidt, G.L.; Falgout, J.T.; Williams, B.; Fairaux, N.M.; Caldwell, M.K.; Picotte, J.J.; et al. Mapping Burned areas Using Dense Time-Series of Landsat Data. *Remote Sens. Environ.* **2017**, *198*, 504–522. [CrossRef]
80. Liu, J.; Heiskanen, J.; Maeda, E.E.; Pellikka, P.K.E. Burned area Detection Based on Landsat Time Series in Savannas of Southern Burkina Faso. *Int. J. Appl. Earth Obs. Geoinf.* **2018**, *64*, 210–220. [CrossRef]
81. Long, T.; Zhang, Z.; He, G.; Jiao, W.; Tang, C.; Wu, B.; Zhang, X.; Wang, G.; Yin, R. 30 m Resolution Global Annual Burned area Mapping Based on Landsat Images and Google Earth Engine. *Remote Sens.* **2019**, *11*, 489. [CrossRef]
82. Woodcock, C.E.; Allen, R.; Anderson, M.; Belward, A.; Bindschadler, R.; Cohen, W.; Gao, F.; Goward, S.N.; Helder, D.; Helmer, E.; et al. Free Access to Landsat Imagery. *Science* **2008**, *320*, 1011. [CrossRef]
83. Wulder, M.A.; White, J.C.; Loveland, T.R.; Woodcock, C.E.; Belward, A.S.; Cohen, W.B.; Fosnight, E.A.; Shaw, J.; Masek, J.G.; Roy, D.P. The Global Landsat Archive: Status, Consolidation, and Direction. *Remote Sens. Environ.* **2016**, *185*, 271–283. [CrossRef]
84. Loveland, T.R.; Dwyer, J.L. Landsat: Building a Strong Future. *Remote Sens. Environ.* **2012**, *122*, 22–29. [CrossRef]
85. Hardtke, L.A.; Blanco, P.D.; del Valle, H.F.; Metternicht, G.I.; Sione, W.F. Automated Mapping of Burned areas in Semi-Arid Ecosystems Using Modis Time-Series Imagery. *Int. Arch. Photogramm. Remote Sens. Spat. Inf. Sci.* **2015**, *XL-7/W3*, 811–814. [CrossRef]
86. Silva, J.M.N.; Moreno, M.V.; Le Page, Y.; Oom, D.; Bistinas, I.; Pereira, J.M.C. Spatiotemporal Trends of Area Burnt in the Iberian Peninsula, 1975–2013. *Reg. Environ. Change* **2019**, *19*, 515–527. [CrossRef]
87. Alencar, A.A.C.; Arruda, V.L.S.; da Silva, W.V.; Conciani, D.E.; Costa, D.P.; Crusco, N.; Duverger, S.G.; Ferreira, N.C.; Franca-Rocha, W.; Hasenack, H.; et al. Long-Term Landsat-Based Monthly Burned area Dataset for the Brazilian Biomes Using Deep Learning. *Remote Sens.* **2022**, *14*, 2510. [CrossRef]
88. Neves, A.K.; Campagnolo, M.L.; Silva, J.M.N.; Pereira, J.M.C. A Landsat-Based Atlas of Monthly Burned area for Portugal, 1984–2021. *Int. J. Appl. Earth Obs. Geoinf.* **2023**, *119*, 103321. [CrossRef]
89. Roy, D.P.; Huang, H.; Boschetti, L.; Giglio, L.; Yan, L.; Zhang, H.H.; Li, Z. Landsat-8 and Sentinel-2 Burned area Mapping—A Combined Sensor Multi-Temporal Change Detection Approach. *Remote Sens. Environ.* **2019**, *231*, 111254. [CrossRef]
90. Melchiorre, A.; Boschetti, L. Global Analysis of Burned area Persistence Time with MODIS Data. *Remote Sens.* **2018**, *10*, 750. [CrossRef]
91. Pereira, J.M.C. Remote Sensing of Burned areas in Tropical Savannas. *Int. J. Wildland Fire* **2003**, *12*, 259. [CrossRef]
92. Trigg, S.; Flasse, S. Characterizing the Spectral-Temporal Response of Burned Savannah Using in Situ Spectroradiometry and Infrared Thermometry. *Int. J. Remote Sens.* **2000**, *21*, 3161–3168. [CrossRef]
93. Ngadze, F.; Mpakairi, K.S.; Kavhu, B.; Ndaimani, H.; Maremba, M.S. Exploring the Utility of Sentinel-2 MSI and Landsat 8 OLI in Burned area Mapping for a Heterogenous Savannah Landscape. *PLoS ONE* **2020**, *15*, e0232962. [CrossRef]
94. Mpakairi, K.S.; Ndaimani, H.; Kavhu, B. Exploring the Utility of Sentinel-2 MSI Derived Spectral Indices in Mapping Burned areas in Different Land-Cover Types. *Sci. Afr.* **2020**, *10*, e00565. [CrossRef]
95. Gülci, S.; Yüksel, K.; Gümüş, S.; Wing, M. Mapping Wildfires Using Sentinel 2 MSI and Landsat 8 Imagery: Spatial Data Generation for Forestry. *Eur. J. For. Eng.* **2021**, *7*, 57–66. [CrossRef]
96. Verhegghen, A.; Eva, H.; Ceccherini, G.; Achard, F.; Gond, V.; Gourlet-Fleury, S.; Cerutti, P. The Potential of Sentinel Satellites for Burned area Mapping and Monitoring in the Congo Basin Forests. *Remote Sens.* **2016**, *8*, 986. [CrossRef]

97. Huang, H.; Roy, D.; Boschetti, L.; Zhang, H.; Yan, L.; Kumar, S.; Gomez-Dans, J.; Li, J. Separability Analysis of Sentinel-2A Multi-Spectral Instrument (MSI) Data for Burned area Discrimination. *Remote Sens.* **2016**, *8*, 873. [CrossRef]
98. Fernández-Manso, A.; Fernández-Manso, O.; Quintano, C. SENTINEL-2A Red-Edge Spectral Indices Suitability for Discriminating Burn Severity. *Int. J. Appl. Earth Obs. Geoinf.* **2016**, *50*, 170–175. [CrossRef]
99. Amos, C.; Petropoulos, G.P.; Ferentinos, K.P. Determining the Use of Sentinel-2A MSI for Wildfire Burning & Severity Detection. *Int. J. Remote Sens.* **2019**, *40*, 905–930. [CrossRef]
100. Li, J.; Roy, D. A Global Analysis of Sentinel-2A, Sentinel-2B and Landsat-8 Data Revisit Intervals and Implications for Terrestrial Monitoring. *Remote Sens.* **2017**, *9*, 902. [CrossRef]
101. Santana, N.C.; De Carvalho Júnior, O.A.; Gomes, R.A.T.; Guimarães, R.F. Burned-Area Detection in Amazonian Environments Using Standardized Time Series Per Pixel in MODIS Data. *Remote Sens.* **2018**, *10*, 1904. [CrossRef]
102. Bastarrika, A.; Rodriguez-Montellano, A.; Roteta, E.; Hantson, S.; Franquesa, M.; Torre, L.; Gonzalez-Ibarzabal, J.; Artano, K.; Martinez-Blanco, P.; Mesanza, A.; et al. An Automatic Procedure for Mapping Burned areas Globally Using Sentinel-2 and VIIRS/MODIS Active Fires in Google Earth Engine. *ISPRS J. Photogramm. Remote Sens.* **2024**, *218*, 232–245. [CrossRef]
103. Kouachi, M.E.; Khairoun, A.; Moghli, A.; Rahmani, S.; Mouillot, F.; Baeza, M.J.; Moutahir, H. Forty-Year Fire History Reconstruction from Landsat Data in Mediterranean Ecosystems of Algeria Following International Standards. *Remote Sens.* **2024**, *16*, 2500. [CrossRef]
104. Parks, S.; Dillon, G.; Miller, C. A New Metric for Quantifying Burn Severity: The Relativized Burn Ratio. *Remote Sens.* **2014**, *6*, 1827–1844. [CrossRef]
105. Veraverbeke, S.; Hook, S.; Hulley, G. An Alternative Spectral Index for Rapid Fire Severity Assessments. *Remote Sens. Environ.* **2012**, *123*, 72–80. [CrossRef]
106. De Santis, A.; Asner, G.P.; Vaughan, P.J.; Knapp, D.E. Mapping Burn Severity and Burning Efficiency in California Using Simulation Models and Landsat Imagery. *Remote Sens. Environ.* **2010**, *114*, 1535–1545. [CrossRef]
107. Fotakidis, V.; Chrysafis, I.; Mallinis, G.; Koutsias, N. Continuous Burned area Monitoring Using Bi-Temporal Spectral Index Time Series Analysis. *Int. J. Appl. Earth Obs. Geoinf.* **2023**, *125*, 103547. [CrossRef]
108. Xulu, S.; Mbatha, N.; Peerbhay, K. Burned area Mapping over the Southern Cape Forestry Region, South Africa Using Sentinel Data within GEE Cloud Platform. *ISPRS Int. J. Geoinf.* **2021**, *10*, 511. [CrossRef]
109. De Carvalho Júnior, O.; Guimarães, R.; Silva, C.; Gomes, R. Standardized Time-Series and Interannual Phenological Deviation: New Techniques for Burned-Area Detection Using Long-Term MODIS-NBR Dataset. *Remote Sens.* **2015**, *7*, 6950–6985. [CrossRef]
110. Trigg, S.; Flasse, S. An Evaluation of Different Bi-Spectral Spaces for Discriminating Burned Shrub-Savannah. *Int. J. Remote Sens.* **2001**, *22*, 2641–2647. [CrossRef]
111. Steel, Z.L.; Safford, H.D.; Viers, J.H. The Fire Frequency-severity Relationship and the Legacy of Fire Suppression in California Forests. *Ecosphere* **2015**, *6*, 1–23. [CrossRef]
112. Navarro, G.; Caballero, I.; Silva, G.; Parra, P.-C.; Vázquez, Á.; Caldeira, R. Evaluation of Forest Fire on Madeira Island Using Sentinel-2A MSI Imagery. *Int. J. Appl. Earth Obs. Geoinf.* **2017**, *58*, 97–106. [CrossRef]
113. Solarna, D.; Moser, G.; Serpico, S.B. A Markovian Approach to Unsupervised Change Detection with Multiresolution and Multimodality SAR Data. *Remote Sens.* **2018**, *10*, 1671. [CrossRef]
114. Yousif, O.; Ban, Y. Improving SAR-Based Urban Change Detection by Combining MAP-MRF Classifier and Nonlocal Means Similarity Weights. *IEEE J. Sel. Top. Appl. Earth Obs. Remote Sens.* **2014**, *7*, 4288–4300. [CrossRef]
115. Chen, Y.; Cao, Z. An Improved MRF-Based Change Detection Approach for Multitemporal Remote Sensing Imagery. *Signal Process.* **2013**, *93*, 163–175. [CrossRef]
116. Bruzzone, L.; Prieto, D.F. Automatic Analysis of the Difference Image for Unsupervised Change Detection. *IEEE Trans. Geosci. Remote Sens.* **2000**, *38*, 1171–1182. [CrossRef]
117. Bruzzone, L.; Prieto, D.F. An Adaptive Semiparametric and Context-Based Approach to Unsupervised Change Detection in Multitemporal Remote-Sensing Images. *IEEE Trans. Image Process.* **2002**, *11*, 452–466. [CrossRef] [PubMed]
118. Benedek, C.; Sziranyi, T. Change Detection in Optical Aerial Images by a Multilayer Conditional Mixed Markov Model. *IEEE Trans. Geosci. Remote Sens.* **2009**, *47*, 3416–3430. [CrossRef]
119. Tso, B.; Olsen, R.C. A Contextual Classification Scheme Based on MRF Model with Improved Parameter Estimation and Multiscale Fuzzy Line Process. *Remote Sens. Environ.* **2005**, *97*, 127–136. [CrossRef]
120. Smits, P.C.; Dellepiane, S.G. Synthetic Aperture Radar Image Segmentation by a Detail Preserving Markov Random Field Approach. *IEEE Trans. Geosci. Remote Sens.* **1997**, *35*, 844–857. [CrossRef]
121. Garzelli, A. Classification of Polarimetric SAR Images Using Adaptive Neighbourhood Structures. *Int. J. Remote Sens.* **1999**, *20*, 1669–1675. [CrossRef]
122. Tassi, A.; Gil, A. A Low-Cost Sentinel-2 Data and Rao's Q Diversity Index-Based Application for Detecting, Assessing and Monitoring Coastal Land-Cover/Land-Use Changes at High Spatial Resolution. *J. Coast. Res.* **2020**, *95*, 1315. [CrossRef]

123. Tassi, A.; Massetti, A.; Gil, A. The Spectralrao-Monitoring Python Package: A RAO's Q Diversity Index-Based Application for Land-Cover/Land-Use Change Detection in Multifunctional Agricultural Areas. *Comput. Electron. Agric.* **2022**, *196*, 106861. [CrossRef]
124. Rocchini, D.; Marcantonio, M.; Ricotta, C. Measuring Rao's Q Diversity Index from Remote Sensing: An Open Source Solution. *Ecol. Indic.* **2017**, *72*, 234–238. [CrossRef]
125. Tiengo, R.; Merino-De-Miguel, S.; Uchôa, J.; Gil, A. A Land Cover Change Detection Approach to Assess the Effectiveness of Conservation Projects: A Study Case on the EU-Funded LIFE Projects in São Miguel Island, Azores (2002–2021). *Land* **2024**, *13*, 666. [CrossRef]
126. Purdon, A.; Mole, M.A.; Selier, J.; Kruger, J.; Mafumo, H.; Olivier, P.I. Using the Rao's Q Diversity Index as an Indicator of Protected Area Effectiveness in Conserving Biodiversity. *Ecol. Inform.* **2022**, *72*, 101920. [CrossRef]
127. Filipponi, F. BAIS2: Burned area Index for Sentinel-2. *Proceedings* **2018**, *2*, 364. [CrossRef]
128. Salis, M.; Ager, A.A.; Alcasena, F.J.; Arca, B.; Finney, M.A.; Pellizzaro, G.; Spano, D. Analyzing Seasonal Patterns of Wildfire Exposure Factors in Sardinia, Italy. *Environ. Monit. Assess.* **2015**, *187*, 4175. [CrossRef]
129. Schwörer, C.; Morales-Molino, C.; Gobet, E.; Henne, P.D.; Pasta, S.; Pedrotta, T.; van Leeuwen, J.F.N.; Vannière, B.; Tinner, W. Simulating Past and Future Fire Impacts on Mediterranean Ecosystems. *J. Ecol.* **2024**, *112*, 954–970. [CrossRef]
130. Scarpa, C.; Elia, M.; D'Este, M.; Salis, M.; Rodrigues, M.; Arca, B.; Duce, P.; Fiori, M.A.F.; Pellizzaro, G. Modelling Wildfire Activity in Wildland–Urban Interface (WUI) Areas of Sardinia, Italy. *Int. J. Wildland Fire* **2024**, *33*, 1–16. [CrossRef]
131. Quave, C.L.; Saitta, A. Forty-Five Years Later: The Shifting Dynamic of Traditional Ecological Knowledge on Pantelleria Island, Italy. *Econ. Bot.* **2016**, *70*, 380–393. [CrossRef]
132. Fichera, G.; Mucedda, M.; Russo, D.; Tomassini, A.; Kiefer, A.; Veith, M.; Ancillotto, L. Pantelleria Island (Sicily, Italy): A Biogeographic Crossroad for Bats between Africa and Europe. *Hystrix Ital. J. Mammal.* **2022**, *33*, 134–137.
133. Sakellariou, S.; Parisien, M.-A.; Flannigan, M.; Wang, X.; de Groot, B.; Tampekis, S.; Samara, F.; Sfougaris, A.; Christopoulou, O. Spatial Planning of Fire-Agency Stations as a Function of Wildfire Likelihood in Thasos, Greece. *Sci. Total Environ.* **2020**, *729*, 139004. [CrossRef]
134. Gitas, I.Z.; Devereux, B.J. The Role of Topographic Correction in Mapping Recently Burned Mediterranean Forest Areas from LANDSAT TM Images. *Int. J. Remote Sens.* **2006**, *27*, 41–54. [CrossRef]
135. Calò, C.; Henne, P.D.; Eugster, P.; van Leeuwen, J.; Gilli, A.; Hamann, Y.; La Mantia, T.; Pasta, S.; Vescovi, E.; Tinner, W. 1200 Years of Decadal-Scale Variability of Mediterranean Vegetation and Climate at Pantelleria Island, Italy. *Holocene* **2013**, *23*, 1477–1486. [CrossRef]
136. Lasaponara, R. Estimating Spectral Separability of Satellite Derived Parameters for Burned areas Mapping in the Calabria Region by Using SPOT-Vegetation Data. *Ecol. Model.* **2006**, *196*, 265–270. [CrossRef]
137. Soverel, N.O.; Perrakis, D.D.B.; Coops, N.C. Estimating Burn Severity from Landsat DNBR and RdNBR Indices across Western Canada. *Remote Sens. Environ.* **2010**, *114*, 1896–1909. [CrossRef]
138. CEMS EMSR371: Fire in Sardinia, Italy. Available online: https://emergency.copernicus.eu/mapping/list-of-components/EMSR371 (accessed on 10 July 2024).
139. CEMS EMSR624: Forest Fire in Thassos Island—Greece. Available online: https://emergency.copernicus.eu/mapping/list-of-components/EMSR624 (accessed on 10 July 2024).
140. CEMS EMSR626: Wildfire in Pantelleria Island, Italy. Available online: https://emergency.copernicus.eu/mapping/list-of-components/EMSR626 (accessed on 10 July 2024).
141. van Dijk, D.; Shoaie, S.; van Leeuwen, T.; Veraverbeke, S. Spectral Signature Analysis of False Positive Burned area Detection from Agricultural Harvests Using Sentinel-2 Data. *Int. J. Appl. Earth Obs. Geoinf.* **2021**, *97*, 102296. [CrossRef]
142. Pacheco, A.D.P.; da Silva Junior, J.A.; Ruiz-Armenteros, A.M.; Henriques, R.F.F.; de Oliveira Santos, I. Analysis of Spectral Separability for Detecting Burned areas Using Landsat-8 OLI/TIRS Images under Different Biomes in Brazil and Portugal. *Forests* **2023**, *14*, 663. [CrossRef]
143. Rouse, J.; Haas, R.H.; Schell, J.A.; Deering, D.W. *Monitoring Vegetation Systems in the Great Plains with ERTS*; NASA: Washington, DC, USA, 1974.
144. Chuvieco, E.; Martín, M.P.; Palacios, A. Assessment of Different Spectral Indices in the Red-near-Infrared Spectral Domain for Burned Land Discrimination. *Int. J. Remote Sens.* **2002**, *23*, 5103–5110. [CrossRef]
145. Roy, D.P.; Boschetti, L.; Trigg, S.N. Remote Sensing of Fire Severity: Assessing the Performance of the Normalized Burn Ratio. *IEEE Geosci. Remote Sens. Lett.* **2006**, *3*, 112–116. [CrossRef]
146. Tiengo, R.; Palácios-Orueta, A.; Uchôa, J.; Gil, A. Remote Sensing Approaches for Land Use/Land Cover Change in Coastal Areas and Oceanic Islands: An Open Science-Based Systematic Review. *Rev. Gestão Costeira Integr.* **2023**, *23*, 155–177. [CrossRef]
147. Tucker, C.J. Red and Photographic Infrared Linear Combinations for Monitoring Vegetation. *Remote Sens. Environ.* **1979**, *8*, 127–150. [CrossRef]

148. Sivrikaya, F.; Günlü, A.; Küçük, Ö.; Ürker, O. Forest Fire Risk Mapping with Landsat 8 OLI Images: Evaluation of the Potential Use of Vegetation Indices. *Ecol. Inform.* **2024**, *79*, 102461. [CrossRef]
149. Rakholia, S.; Mehta, A.; Suthar, B. Forest Fire Monitoring of Shoolpaneshwar Wildlife Sanctuary, Gujarat, India Using Geospatial Techniques. *Curr. Sci.* **2020**, *119*, 1974. [CrossRef]
150. Uchôa, J.; Viveiros, F.; Tiengo, R.; Gil, A. Detection of Geothermal Anomalies in Hydrothermal Systems Using ASTER Data: The Caldeiras Da Ribeira Grande Case Study (Azores, Portugal). *Sensors* **2023**, *23*, 2258. [CrossRef] [PubMed]
151. Zhao, Y.; Huang, Y.; Sun, X.; Dong, G.; Li, Y.; Ma, M. Forest Fire Mapping Using Multi-Source Remote Sensing Data: A Case Study in Chongqing. *Remote Sens.* **2023**, *15*, 2323. [CrossRef]
152. Key, C.; Benson, N. *Landscape Assessment: Ground Measure of Severity, the Composite Burn Index; and Remote Sensing of Severity, the Normalized Burn Ratio*; USDA Forest Service: Ogden, UT, USA, 2005.
153. Marín-Ortiz, J.C.; Gutierrez-Toro, N.; Botero-Fernández, V.; Hoyos-Carvajal, L.M. Linking Physiological Parameters with Visible/near-Infrared Leaf Reflectance in the Incubation Period of Vascular Wilt Disease. *Saudi J. Biol Sci.* **2020**, *27*, 88–99. [CrossRef] [PubMed]
154. Zidane, I.; Lhissou, R.; Bouli, A.; Mabrouki, M. An Improved Algorithm for Mapping Burned areas in the Mediterranean Forest Landscape of Morocco. *J. For. Res.* **2019**, *30*, 981–992. [CrossRef]
155. Storey, E.A.; Lee West, K.R.; Stow, D.A. Utility and Optimization of LANDSAT-Derived Burned area Maps for Southern California. *Int. J. Remote Sens.* **2021**, *42*, 486–505. [CrossRef]
156. Rocchini, D.; Marcantonio, M.; Da Re, D.; Bacaro, G.; Feoli, E.; Foody, G. From Zero to Infinity: Minimum to Maximum Diversity of the Planet by Spatio-Parametric Rao's Quadratic Entropy. *Glob. Ecol. Biogeogr.* **2021**, *30*, 1153–1162. [CrossRef]
157. Rocchini, D.; Torresani, M.; Ricotta, C. On the Mathematical Properties of Spatial Rao's Q to Compute Ecosystem Heterogeneity. *Theor. Ecol.* **2024**, *17*, 247–254. [CrossRef]
158. Shivakumar, B.R.; Rajashekararadhya, S.V. An Investigation on Land Cover Mapping Capability of Classical and Fuzzy Based Maximum Likelihood Classifiers. *Int. J. Eng. Technol.* **2018**, *7*, 939. [CrossRef]
159. Richards, J.A. *Remote Sensing Digital Image Analysis*, 5th ed.; Richards, J.A., Ed.; Springer: Berlin/Heidelberg, Germany, 2013; 494p, ISBN 978-3-642-30062-2.
160. Okwuashi, O.; Isong, M.; Eyo, E.; Eyoh, A.; Nwanekezie, O.; Olayinka, D.N.; Udoudo, D.O.; Ofem, B. GIS Cellular Automata Using Artificial Neural Network for Land Use Change Simulation of Lagos, Nigeria. *J. Geogr. Geol.* **2012**, *4*, 94–101. [CrossRef]
161. Foody, G.M. Explaining the Unsuitability of the Kappa Coefficient in the Assessment and Comparison of the Accuracy of Thematic Maps Obtained by Image Classification. *Remote Sens. Environ.* **2020**, *239*, 111630. [CrossRef]
162. van Vliet, J.; Bregt, A.K.; Hagen-Zanker, A. Revisiting Kappa to Account for Change in the Accuracy Assessment of Land-Use Change Models. *Ecol. Model.* **2011**, *222*, 1367–1375. [CrossRef]
163. Allouche, O.; Tsoar, A.; Kadmon, R. Assessing the Accuracy of Species Distribution Models: Prevalence, Kappa and the True Skill Statistic (TSS). *J. Appl. Ecol.* **2006**, *43*, 1223–1232. [CrossRef]
164. Olofsson, P.; Foody, G.M.; Herold, M.; Stehman, S.V.; Woodcock, C.E.; Wulder, M.A. Good Practices for Estimating Area and Assessing Accuracy of Land Change. *Remote Sens. Environ.* **2014**, *148*, 42–57. [CrossRef]
165. Foody, G.M. Status of Land Cover Classification Accuracy Assessment. *Remote Sens. Environ.* **2002**, *80*, 185–201. [CrossRef]
166. Stehman, S.V.; Foody, G.M. Key Issues in Rigorous Accuracy Assessment of Land Cover Products. *Remote Sens. Environ.* **2019**, *231*, 111199. [CrossRef]
167. Foody, G.M. Assessing the Accuracy of Land Cover Change with Imperfect Ground Reference Data. *Remote Sens. Environ.* **2010**, *114*, 2271–2285. [CrossRef]
168. Fitzgerald, R.W.; Lees, B.G. Assessing the Classification Accuracy of Multisource Remote Sensing Data. *Remote Sens. Environ.* **1994**, *47*, 362–368. [CrossRef]
169. Cohen, J. A Coefficient of Agreement for Nominal Scales. *Educ. Psychol. Meas.* **1960**, *20*, 37–46. [CrossRef]
170. Pontius, R.G.; Millones, M. Death to Kappa: Birth of Quantity Disagreement and Allocation Disagreement for Accuracy Assessment. *Int. J. Remote Sens.* **2011**, *32*, 4407–4429. [CrossRef]
171. Coetzee, B.W.T.; Robertson, M.P.; Erasmus, B.F.N.; Van Rensburg, B.J.; Thuiller, W. Ensemble Models Predict Important Bird Areas in Southern Africa Will Become Less Effective for Conserving Endemic Birds under Climate Change. *Glob. Ecol. Biogeogr.* **2009**, *18*, 701–710. [CrossRef]
172. Pérez, C.C.; Olthoff, A.E.; Hernández-Trejo, H.; Rullán-Silva, C.D. Evaluating the Best Spectral Indices for Burned areas in the Tropical Pantanos de Centla Biosphere Reserve, Southeastern Mexico. *Remote Sens. Appl.* **2022**, *25*, 100664. [CrossRef]
173. Schepers, L.; Haest, B.; Veraverbeke, S.; Spanhove, T.; Vanden Borre, J.; Goossens, R. Burned area Detection and Burn Severity Assessment of a Heathland Fire in Belgium Using Airborne Imaging Spectroscopy (APEX). *Remote Sens.* **2014**, *6*, 1803–1826. [CrossRef]
174. Lu, B.; He, Y.; Tong, A. Evaluation of Spectral Indices for Estimating Burn Severity in Semiarid Grasslands. *Int. J. Wildland Fire* **2016**, *25*, 147. [CrossRef]

175. Fornacca, D.; Ren, G.; Xiao, W. Evaluating the Best Spectral Indices for the Detection of Burn Scars at Several Post-Fire Dates in a Mountainous Region of Northwest Yunnan, China. *Remote Sens.* **2018**, *10*, 1196. [CrossRef]
176. Epting, J.; Verbyla, D.; Sorbel, B. Evaluation of Remotely Sensed Indices for Assessing Burn Severity in Interior Alaska Using Landsat TM and ETM+. *Remote Sens. Environ.* **2005**, *96*, 328–339. [CrossRef]
177. White, J.; Ryan, K.; Key, C.; Running, S. Remote Sensing of Forest Fire Severity and Vegetation Recovery. *Int. J. Wildland Fire* **1996**, *6*, 125. [CrossRef]
178. Roy, D.P. Multi-Temporal Active-Fire Based Burn Scar Detection Algorithm. *Int. J. Remote Sens.* **1999**, *20*, 1031–1038. [CrossRef]
179. Harris, S.; Veraverbeke, S.; Hook, S. Evaluating Spectral Indices for Assessing Fire Severity in Chaparral Ecosystems (Southern California) Using MODIS/ASTER (MASTER) Airborne Simulator Data. *Remote Sens.* **2011**, *3*, 2403–2419. [CrossRef]
180. Han, A.; Qing, S.; Bao, Y.; Na, L.; Bao, Y.; Liu, X.; Zhang, J.; Wang, C. Short-Term Effects of Fire Severity on Vegetation Based on Sentinel-2 Satellite Data. *Sustainability* **2021**, *13*, 432. [CrossRef]
181. Smiraglia, D.; Filipponi, F.; Mandrone, S.; Tornato, A.; Taramelli, A. Agreement Index for Burned area Mapping: Integration of Multiple Spectral Indices Using Sentinel-2 Satellite Images. *Remote Sens.* **2020**, *12*, 1862. [CrossRef]